



SPITZER OBSERVATIONS OF LONG-TERM INFRARED VARIABILITY AMONG YOUNG STELLAR OBJECTS IN CHAMAELEON I

KEVIN M. FLAHERTY¹, LINDSAY DEMARCHI^{2,3}, JAMES MUZEROLLE⁴, ZOLTAN BALOG⁵, WILLIAM HERBST¹,
S. THOMAS MEGEATH⁶, ELISE FURLAN⁷, AND ROBERT GUTERMUTH⁸

¹ Van Vleck Observatory, Astronomy Department, Wesleyan University, 96 Foss Hill Drive, Middletown, CT 06459, USA

² Department of Physics and Astronomy, Colgate University, 13 Oak Drive, Hamilton, NY 13346, USA

³ Department of Physics, Syracuse University, Syracuse, NY, 13244, USA

⁴ Space Telescope Science Institute, 3700 San Martin Drive, Baltimore, MD 21218, USA

⁵ Max-Planck-Institut für Astronomie, Königstuhl 17, D-69117 Heidelberg, Germany

⁶ Ritter Astrophysical Research Center, Department of Physics and Astronomy, University of Toledo, Toledo, OH 43606, USA

⁷ Infrared Processing and Analysis Center, California Institute of Technology, 770 S. Wilson Avenue, Pasadena, CA 91125, USA

⁸ Department of Astronomy, University of Massachusetts, Amherst, MA 01003, USA

Received 2016 June 29; revised 2016 September 27; accepted 2016 September 27; published 2016 December 9

ABSTRACT

Infrared variability is common among young stellar objects, with surveys finding daily to weekly fluctuations of a few tenths of a magnitude. Space-based observations can produce highly sampled infrared light curves, but are often limited to total baselines of about 1 month due to the orientation of the spacecraft. Here we present observations of the Chameleon I cluster, whose low declination makes it observable by the *Spitzer Space Telescope* over a 200-day period. We observe 30 young stellar objects with a daily cadence to better sample variability on timescales of months. We find that such variability is common, occurring in $\sim 80\%$ of the detected cluster members. The change in $[3.6]-[4.5]$ color over 200 days for many of the sources falls between that expected for extinction and fluctuations in disk emission. With our high cadence and long baseline we can derive power spectral density curves covering two orders of magnitude in frequency and find significant power at low frequencies, up to the boundaries of our 200-day survey. Such long timescales are difficult to explain with variations driven by the interaction between the disk and stellar magnetic field, which has a dynamical timescale of days to weeks. The most likely explanation is either structural or temperature fluctuations spread throughout the inner ~ 0.5 au of the disk, suggesting that the intrinsic dust structure is highly dynamic.

Key words: accretion, accretion disks – protoplanetary disks – stars: pre-main sequence

Supporting material: figure set

1. INTRODUCTION

In young stellar objects (YSOs) the inner disk ($\lesssim 1$ au) stands at the intersection between gas, dust, and the star itself. The gas disk is truncated by its interaction with the stellar magnetic field (~ 0.05 au), while the dust disk inner edge occurs where the grains are heated to a high enough temperature to sublimate (0.1–1 au). The exact structure can be difficult to study given the small size of these regions, making resolved observations challenging, although not impossible (e.g., Menu et al. 2015; Millan-Gabet et al. 2016). Unresolved observations have been successful in revealing the general structure of this region. Spectral line profiles trace the free fall of gas onto the stellar surface along magnetic field lines after it is lifted away from the disk (e.g., Lima et al. 2010), as well as outflows (Edwards et al. 2013; Cauley & Johns-Krull 2015). Infrared observations find strong emission from $T \sim 1500$ K dust (e.g., McClure et al. 2013a), consistent with a curved inner wall (Isella & Natta 2005; Flock et al. 2016). Recent studies have found evidence for multiple populations of dust grains with different inner radii (McClure et al. 2013b), consistent with the expectation that small dust grains reach the sublimation temperature farther from the star because they more efficiently absorb the stellar irradiation. While here we focus on the dust, much has been learned about the gas structure within this region (see reviews by Bouvier et al. 2007; Dullemond & Monnier 2010).

Variability serves as an additional tool for studying the inner disk. Recent surveys have found that the vast majority of YSOs

are variable in the mid-infrared on timescales of days to weeks (Cody et al. 2014; Rebull et al. 2014), expanding on earlier ground-based near-infrared studies (e.g., Carpenter et al. 2001). These surveys have also revealed additional clues as to the structure of the inner disk. Meng et al. (2016) use reverberation mapping to derive the location of the dust inner wall. Espaillat et al. (2011) demonstrate that the wavelength dependence of the variability in pre-transition disks, systems with an optically thick inner disk followed by an optically thin gap and an optically thick outer disk, can be explained by varying the height of the inner disk, indicating that this region is not static. McGinnis et al. (2015) find, based on quasi-periodic occultations of the stellar surface, that the height of the inner wall can vary by $\sim 10\%$ over short timescales even in full disks. Bouvier et al. (2003) find that the variability of AA Tau is consistent with periodic occultations by a warped inner disk. Such nonaxisymmetric structure is difficult to study with spatially unresolved observations, which often rely on fits to axisymmetric models.

Most previous *Spitzer* time domain studies of YSOs were restricted to baselines of 1–2 months due to the duration of a single visibility window for most star-forming regions, while ground-based near-infrared studies have found variability extending out to year-long timescales (Wolk et al. 2013; Parks et al. 2014), although with a sparser cadence than is possible with space-based observatories. Long timescales push toward larger radii in the disk; if the timescale of the variability is proportional to the local Keplerian period, then year-long

fluctuations imply variability at ~ 1 au from the central star. A detailed characterization of long-timescale variability can improve our understanding of this important planet-forming region of the disk.

Here we probe variability over weeks to months using *Spitzer Space Telescope* observations of the Chamaeleon I (Cha I) star-forming region (Luhman 2008). Due to its low declination, Cha I can be observed by *Spitzer* over a 200-day window, much longer than the ~ 40 -day windows of other star-forming regions. With photometry (Section 2) taken roughly once per day for 200 days, we produce well-sampled light curves and select out a sample of stars with significant variability (Section 3). We analyze the change in color (Section 4.1) and the timescale of the variability (Section 4.2) and relate this information to potential sources of the variability (Section 5). We find that months-long variability is common and likely due to intrinsic instabilities in disk structure as far out as 0.5 au.

2. DATA

During our survey, we focused on a subset of the young, $d \sim 160$ pc, Cha I low-mass star-forming region (Luhman 2008). Our field of view is located in the northern section of the region (Figure 1) and encompasses over 30 known members, as defined by the samples of Luhman (2007) and Luhman et al. (2008). Membership has been defined using a number of characteristics, including infrared excess emission, spectroscopic properties and extinction (Luhman 2007; Luhman et al. 2008), and proper motions (Lopez Martí et al. 2013). This region was chosen because of its relatively high density of YSOs, allowing us to observe a modest sample in a small area while maximizing the time coverage. Stellar properties are listed in Table 1, with masses estimated using the measured T_{eff} and L_* and the Baraffe et al. (2015) isochrones. Spectral types are taken from Luhman (2008), which agree with more recent surveys (Manara et al. 2016). While the cluster members cover a wide range, from a B9 star down to an M9.5 star, the median star is effectively an early M-type star, with $T_{\text{eff}} = 3400$, $L_* = 0.2 L_{\odot}$ and $M_* = 0.3 M_{\odot}$. While our sample is too small for a detailed comparison, the distribution of stellar masses is consistent with the shape of the initial mass function derived over the entire cluster (Luhman 2007). We draw information on the spectral energy distribution (SED) shape from the analysis of Gutermuth et al. (2009), and where a prior classification was not available we apply the Gutermuth et al. (2009) classification scheme. Accordingly, our sample consists of 3 Class I sources, 24 Class II sources, and 5 Class III sources. None of the previously identified transition disks within Cha I (Kim et al. 2009; Manoj et al. 2011) fall within our field of view.

The focus of our analysis is repeated observations using the IRAC instrument on the *Spitzer Space Telescope* (PID 90141). Both [3.6] and [4.5] images were obtained simultaneously on 200 epochs from 2013 April 16 to 2013 November 07. Each epoch consisted of 12 s HDR exposures with three cycles at each position. The region of interest, centered at 11:10:00, $-76:33:36$, was mapped using a sequence of four pointings, arranged in a 2 by 2 grid, with $260''$ between each pointing. The roughly once-per-day cadence was chosen to cover much of the 220-day long visibility while still tracking the light curve through fluctuations on daily and weekly timescales. Such a low cadence does leave us

relatively insensitive to rapid features, such as short accretion bursts (Stauffer et al. 2014) and “dippers” (e.g., McGinnis et al. 2015). Our focus instead is on the long-term variations that are common (Cody et al. 2014) but difficult to characterize given the ~ 40 -day *Spitzer* observing windows of most previously surveyed regions (e.g., Rebull et al. 2014).

The photometry was derived using the *Spitzer* data reduction pipeline as described in Gutermuth et al. (2009), with updates appropriate for the warm *Spitzer* mission (Morales-Calderón et al. 2012). The uncertainties derived from the images do not include additional systematic uncertainties, and we add systematic uncertainties, derived from the prescription of Cody et al. (2014), in quadrature with statistical uncertainties.

$$\sigma_{\text{sys}} = \begin{cases} \exp^{(m-19.75)} + 0.014 & \text{for [3.6]} \\ \exp^{(m-19.28)} + 0.008 & \text{for [4.5]} \end{cases} \quad (1)$$

$$\sigma^2 = \sigma_{\text{stat}}^2 + \sigma_{\text{sys}}^2 \quad (2)$$

Since most of cluster members are bright, the systematic uncertainties make up the dominant noise component. Selecting sources with $\sigma < 0.1$ mag on at least one epoch in either [3.6] or [4.5], we detect a total of 32 cluster members within our field of view. In addition to these known cluster members, the *Spitzer* field of view includes ~ 1000 other sources, most of which are background or foreground stars unrelated to the Cha I star-forming region. We restrict our analysis to previously discovered cluster members, although additional targets of interest may exist within these data. While we observe the cluster over 200 epochs, we do not have 200 epochs of [3.6] and [4.5] for every cluster member within our field of view (Figure 2). Part of this is due to the incomplete overlap of the [3.6] and [4.5] fields of view, which results in many stars only being observed in one band at a time. Also, during the long visibility window, the spacecraft itself rotates about its axis as it circles the Sun, causing the orientation of the field of view to change with time. The result is that while some stars have coverage from both bands over 200 epochs, many of the cluster members have only partial coverage. Much of the incomplete coverage of any particular source is due to the changing field of view; the stars rarely change flux dramatically enough to either saturate or become too faint for short periods. All but five stars (402, 5073, 6555, 8665, 14260) are detected in both bands, with the median number of detected epochs equal to ~ 100 . This incomplete coverage is accounted for in our analysis.

3. FINDING VARIABLE STARS

The light curves show a wide range of behaviors (Figure 3), with many of the fluctuations appearing stochastic on both short and long timescales. Defining the size of the fluctuations as the difference between the 10th percentile magnitude and the 90th percentile magnitude (Δmag in Table 2), we find fluctuations ranging from 0.05 to 0.5 mag, with a mean of ~ 0.15 , similar to previous surveys (Table 3). We use a combination of statistics to select out variable cluster members in a way that is independent of the exact light-curve shape. We

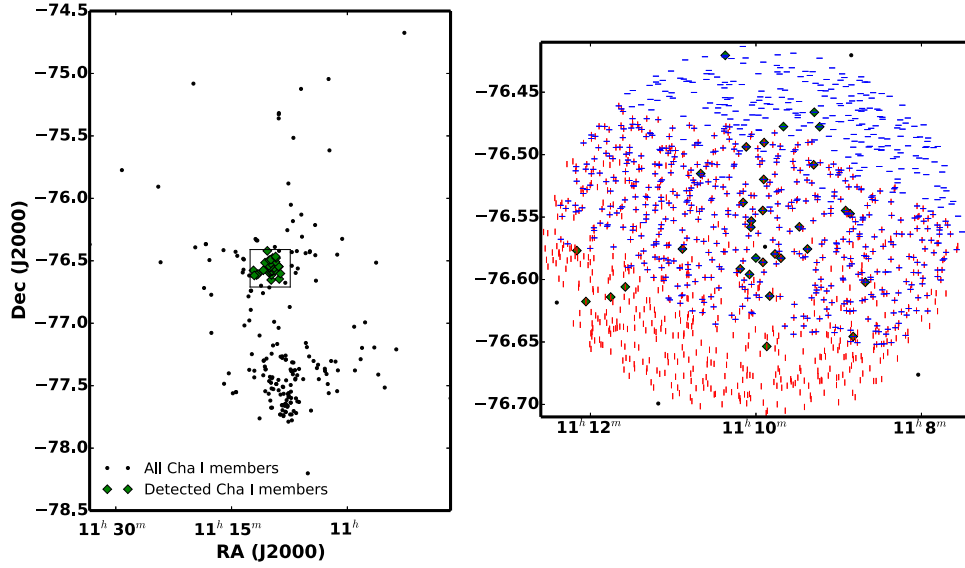


Figure 1. Coverage map comparing the known Cha I cluster members (black dots) with those covered in our survey (green diamonds). The inset shows a close-up on our survey region, with every source detected on more than 20 days in [3.6] (vertical red ticks) and [4.5] (horizontal blue ticks). Our survey focused on a region of Cha I with a relatively high density of YSOs. The rotation of the field of view during the visibility window, as well as the incomplete overlap between the [3.6] and [4.5] fields of view, leads to uneven [3.6] and [4.5] coverage of the cluster.

start with the reduced chi-squared, defined as

$$\chi^2_\nu = \frac{1}{n-1} \sum_{i=1}^n \frac{(m_i - \bar{m})^2}{\sigma_i^2}, \quad (3)$$

to test the hypothesis that the flux is consistent with a constant value defined by the mean. Here n is the number of epochs, m_i is the magnitude in either [3.6] or [4.5] at each epoch, \bar{m} is the mean magnitude, and σ_i is the uncertainty at each epoch. Results for the cluster members are reported in Table 2, and the distribution of chi-squared values, comparing the cluster members with all sources detected in our field of view, at both [3.6] and [4.5] is shown in Figure 4. The majority of noncluster members are nonvariable foreground or background stars whose χ^2_ν peaks at 1, consistent with no significant fluctuations. Among the nonvariable sources, the fluctuations are consistent with white noise, with no evidence of long-term trends or a frequency dependence for the noise over our 200-day observing window. As a boundary between variables and nonvariables, we use $\chi^2_\nu = 3$. Given the brightness of the cluster members, the uncertainties are mostly systematic rather than statistical and are relatively uniform at ~ 0.01 mag, which in turn implies that we are generally sensitive to variations larger than ~ 0.03 mag in both bands. Based on the [3.6] photometry, $74^{+15}_{-20}\%$ (95% confidence interval, 20/27) of the cluster members are variable, while the [4.5] photometry points to $68^{+16}_{-20}\%$ (19/28) of the cluster members as variable. There is a finite probability that a static source could have random fluctuations large enough to result in χ^2_ν , possibly biasing our statistics, and similar studies (e.g., Rebull et al. 2014) have used a χ^2_ν boundary of 5 instead of 3 to eliminate these false positives. Given our small sample size, this does not substantially affect our results; only two stars at [3.6] and one at [4.5] fall within $3 < \chi^2_\nu < 5$. Removing these sources from our sample results in a decrease in the fraction of variable stars that is within our large Poisson errors. The difference

between the fraction of variable stars between the two bands is due entirely to the difference in coverage of the two fields of view; no star is found to be variable in only one channel unless it was only observed in one channel.

The [3.6] and [4.5] flux from young stars with disks traces a region of the SED whose emission is dominated by 1500 K blackbody emission from the inner wall (McClure et al. 2013a), and as a result, we expect the flux in the two bands to be highly correlated. This is seen in previous surveys, with almost no sources exhibiting anticorrelated variability and the most extreme cases showing a small change in [3.6]–[4.5] color (e.g., Cody et al. 2014; Rebull et al. 2014). This correlated behavior can be used to trace variability with the Stetson index (Stetson 1996), which is defined as

$$S = \frac{\sum_{i=1}^n \text{sgn}(P_i) \sqrt{|P_i|}}{N_{\text{pair}}}, \quad (4)$$

where N_{pair} is the number of paired observations, which may or may not be equal to the number of total observations in each band n . The parameter P_i is the product of the normalized residuals in the i th epoch and is defined as

$$P_i = \frac{N_{\text{pair}}}{N_{\text{pair}} - 1} \frac{[3.6]_i - \overline{[3.6]}}{\sigma_{i,[3.6]}} \frac{[4.5]_i - \overline{[4.5]}}{\sigma_{i,[4.5]}}. \quad (5)$$

Figure 5 shows the distribution of Stetson indices for the entire sample, with the cluster members marked. The length of the overlap between [3.6] and [4.5] ranges from 0 to 200 days, with ~ 100 days typical for our sample. We use a boundary of $S > 0.45$ to define variables and find that $80^{+14}_{-24}\%$ (16/20) of the cluster members are variable. All of the sources found to be variable by the Stetson index are also variable based on the chi-squared, while only star 383 is variable based on the [3.6] and [4.5] chi-squared but does not meet our Stetson index threshold. Star 383 has a highly erratic light curve during which there is little overlap between the two bands, which may contribute to its misclassification by the Stetson index. The

Table 1
Stellar Parameters

Index	Name ^a	R.A.	Decl.	Spectral Type	T_{eff} (K)	L_* (L_{\odot})	M_* (M_{\odot})	$\log(\dot{M}$ ($M_{\odot} \text{ yr}^{-1}$))	IR Class	$n_{3.6-4.5}$ ^b	$n_{4.5-24}$ ^b
75	J11095215-7639128	11:09:52.14	-76:39:12.8	M6.25	2962	0.023	0.09	...	II	-0.85 ± 0.11	-0.98 ± 0.02
100	J11084952-7638443	11:08:49.51	-76:38:44.3	M8.75	2478	0.0014	0.07	...	II	-1.43 ± 0.11	-1.07 ± 0.05
239 ^c	J11095003-7636476	11:09:50.01	-76:36:47.7	B9	10500	57	2.6 ^d	...	I	-2.88 ± 0.14	...
299 ^e	J11084069-763078	11:08:40.68	-76:36:07.8	M2.5	3488	0.74	0.4	...	III	-2.71 ± 0.15	-2.84 ± 0.04
330	J11100469-7635452	11:10:04.67	-76:35:45.3	M1	3705	0.43	0.46	$<-9.91^f, -8.87 \pm 0.5^g, -8.9 \pm 0.2^h$	II	-1.93 ± 0.11	-0.87 ± 0.02
360	J11101141-7635292	11:10:11.39	-76:35:29.3	K5.5	4278	1.2	0.9	$-7.98^i, -9.79^f, -9.18 \pm 0.5^g$	II	-1.23 ± 0.11	-0.04 ± 0.01
383	J11095493-7635101	11:09:54.92	-76:35:10.3	M5.75	3024	0.0014	0.17	...	II	-0.7 ± 1.1	-2.1 ± 0.2
402 ^e	J11100010-7634578	11:10:00.08	-76:34:57.9	K5	4350	5.5	1.0	$-6.60^f, -6.6 \pm 0.1^h$	II	0.05 ± 0.11	-0.54 ± 0.01
403	J11094192-7634584	11:09:41.91	-76:34:58.5	<M0	>3850	II	-0.69 ± 0.11	-0.39 ± 0.02
416 ^e	J11094621-7634463	11:09:46.19	-76:34:46.4	M3.25	3379	0.15	0.29	$-8.11^i, -8.3 \pm 0.1^h$	II	-0.53 ± 0.11	-0.21 ± 0.03
439	J11092266-7634320	11:09:22.65	-76:34:32.0	M1.25	3669	0.8	0.4	-7.32^j	II	-0.20 ± 0.11	-0.15 ± 0.01
530	J11100369-7633291	11:10:03.69	-76:33:29.2	K8	3955	0.64	0.63	-8.7 ± 0.3^h	II	-0.24 ± 0.11	-0.57 ± 0.01
533	J11092855-7633281	11:09:28.54	-76:33:28.1	M3.5-M6.5 ^j	3100	1.5	0.1	...	I	3.19 ± 0.15	0.70 ± 0.03
557	J11100336-7633111	11:10:03.35	-76:33:11.1	M4	3270	0.0025	0.25	...	II	-0.07 ± 0.11	0.82 ± 0.02
593	J11085176-7632502	11:08:51.75	-76:32:50.3	M7.25	2838	0.011	0.09	...	II	-2.42 ± 0.15	...
601	J11095505-7632409	11:09:55.04	-76:32:41.0	<M0	>3850	II	0.05 ± 0.11	-0.18 ± 0.02
602	J11085497-7632410	11:08:54.96	-76:32:41.1	M5.5	3058	0.035	0.12	...	II	-1.81 ± 0.11	-1.14 ± 0.02
623	J11100934-7632178	11:10:09.31	-76:32:17.9	M9.5	2300	0.00077	0.075	...	II	-1.35 ± 0.11	-0.59 ± 0.08
691	J11095437-7631113	11:09:54.37	-76:31:11.4	M1.75	3596	0.013	0.35	-10.8 ± 0.4^h	I	0.54 ± 0.15	0.10 ± 0.03
720 ^{e,k}	J11091812-7630292	11:09:18.12	-76:30:29.3	M1.25	3669	0.55	0.43	-7.80^i	II	-0.94 ± 0.11	-0.78 ± 0.01
791 ^e	J11120984-7634366	11:12:09.83	-76:34:36.6	M5	3125	0.15	0.16	...	II	-1.72 ± 0.11	-0.79 ± 0.01
793	J11105333-7634319	11:10:53.32	-76:34:32.0	M3.75	3306	0.13	0.26	$-8.46 \pm 0.5^g, -7.90 \pm 0.6^j$	II	-0.73 ± 0.11	-0.67 ± 0.02
966	J11104006-7630547	11:10:40.05	-76:30:54.7	M7.25	2838	0.0082	0.073	...	II	-2.51 ± 0.15	...
1034 ^{e,m}	J11100704-7629376	11:10:07.03	-76:29:37.7	M0	3850	1.4	0.6	$-8.24 \pm 0.5^g, -8.44 \pm 0.6^j$	II	-1.35 ± 0.11	-0.83 ± 0.01
1103 ^{e,n}	J11094006-7628391	11:09:40.06	-76:28:39.2	M1.25	3669	0.68	0.41	...	II	-3.00 ± 0.15	-2.74 ± 0.03
1504 ^{e,o}	J11095407-7629253	11:09:54.07	-76:29:25.3	M2	3560	0.48	0.36	-7.79^i	II	-1.23 ± 0.11	-0.54 ± 0.02
2712 ^e	J11113474-7636211	11:11:34.73	-76:36:21.2	M2.5	3488	0.21	0.36	...	III	-2.87 ± 0.15	-2.74 ± 0.04
4342	J11114533-7636505	11:11:45.32	-76:36:50.5	M8	2710	0.0033	0.073	...	II	-1.43 ± 0.11	-1.33 ± 0.05
5073	J11120327-7637034	11:12:3.26	-76:37:03.4	M5.5	3058	0.082	0.13	...	III	-2.50 ± 0.15	-2.67 ± 0.08
6555	J11091380-7628396	11:09:13.80	-76:28:39.7	M4.75	3161	0.072	0.18	...	II	-2.55 ± 0.15	-2.74 ± 0.11
8665 ^{e,p}	J11091769-7627578	11:09:17.69	-76:27:57.8	K7	4060	1.1	0.68	...	III	-3.04 ± 0.14	-2.78 ± 0.04
14260	J11102226-7625138	11:10:22.25	-76:25:13.8	M8	2710	0.011	0.076	...	III	-2.59 ± 0.15	...

Notes. Information on the detected cluster members within our sample. Spectral types are taken from Luhman (2008) unless otherwise specified. Masses are estimated using the Baraffe et al. (2015) isochrones unless otherwise noted. Infrared class is taken from Gutermuth et al. (2009) and their classification scheme.

^a Numerous naming conventions have been applied to members of Cha I. Here we list the Two Micron All Sky Survey (2MASS) identifier, and we refer to Luhman (2008) for a more complete list of alternate names.

^b $n_{\lambda_1-\lambda_2} = (\log(\lambda_2 F_{\lambda_2}) - \log(\lambda_1 F_{\lambda_1})) / (\log(\lambda_2) - \log(\lambda_1))$. Photometry taken from Gutermuth et al. (2009) and Luhman et al. (2008).

^c Mass estimate from Siess et al. (2000) isochrones.

^d T41: 0''78 (125 au) binary with B9, M3.5 components (Daemgen et al. 2013).

^e No spectroscopic binary companion detected by Nguyen et al. (2012), with sensitivity down to $\sim 0.1 M_{\odot}$ over 60-day periods.

^f Manara et al. (2016).

^g Frasca et al. (2015).

^h Robberto et al. (2012).

ⁱ Antonucci et al. (2011).

^j Gramajo et al. (2014).

^k CHXR 79: 0''88 (140 au) binary with M2, M4 components (Daemgen et al. 2013).

^l Hartmann et al. (1998).

^m T46: 0''123 (20 au) binary (Lafrenière et al. 2008).

ⁿ CHXR 40: 0''151 (24 au) binary (Lafrenière et al. 2008).

^o T43: 0''78 (126 au) binary with M3.5, M7 components (Daemgen et al. 2013).

^p CHXR 37: 0''079 (13 au) binary (Lafrenière et al. 2008).

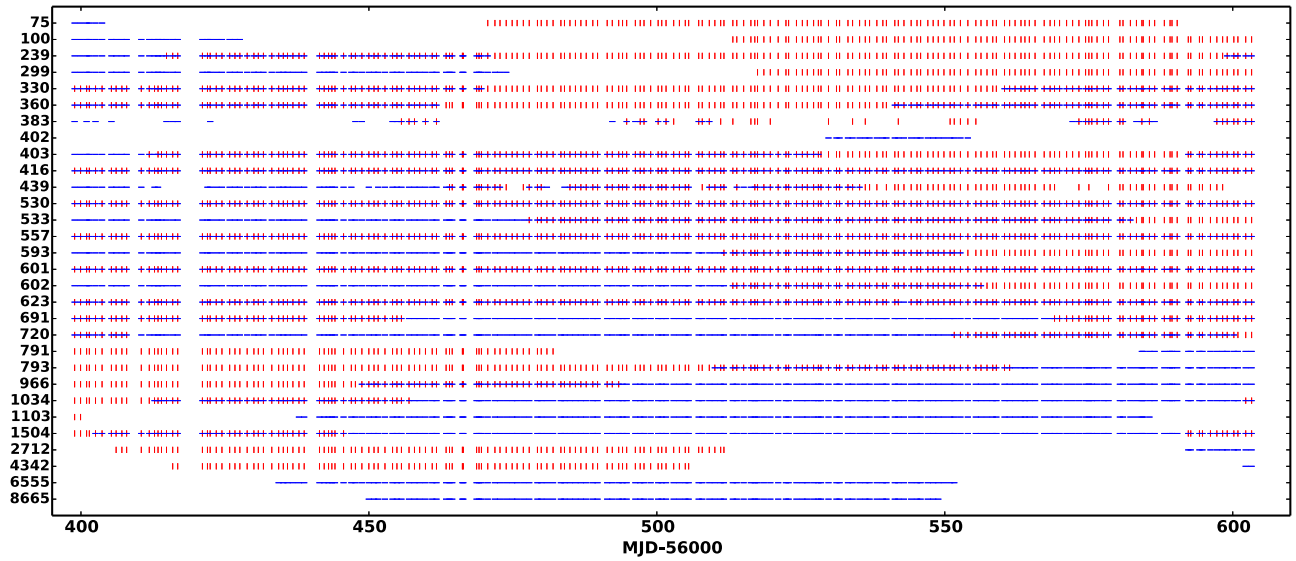


Figure 2. Coverage of the 32 Cha I cluster members in our survey. Vertical red ticks mark observations at [3.6], while horizontal blue ticks mark observations at [4.5]. Due to the rotation of the field of view and the incomplete overlap between the [3.6] and [4.5] fields of view, the time coverage varies between each star and each band.

consistency between the variability detected by the chi-squared and by the Stetson index indicates that the assumption of correlated [3.6] and [4.5] fluctuations does not substantially bias the Stetson index. Our choice of boundary also does not affect our results; similar studies (e.g., Rebull et al. 2014) have used $S > 0.9$, while our weakest variable has $S = 1.5$.

The high fraction of variable stars is consistent with *Spitzer* surveys of infrared variability (Table 3). In particular, the YSOVAR survey, with its *Spitzer* observations of IRAS:20050 +2720 (Poppenhaeger et al. 2015), NGC 1333 (Rebull et al. 2015), the ONC (Morales-Calderón et al. 2011), L1688 (Günther et al. 2014), and GGD 12–15 (Wolk et al. 2015), finds that 60%–85% of YSOs with an infrared excess are variable. Studies of IC 348 (Flaherty et al. 2013), NGC 2264 (Cody et al. 2014), and the Orion molecular cloud (Megeath et al. 2012) have found similar results. Breaking down the sample by SED class, we find that 2/3 Class I objects, 18/24 Class II objects, and 2/5 Class III objects are variable. Previous studies have found infrared variability to be more common among less evolved sources (e.g., Megeath et al. 2012; Flaherty et al. 2013), and our results, while suffering from small number statistics, are marginally consistent with this trend.

4. CHARACTERIZING THE VARIABILITY

Different physical models make different predictions for the properties of the variability. Hot or cold spots on the stellar surface will produce periodic behavior if the spots are long-lived, with a timescale equal to the stellar rotation period, and create fluctuations whose size and color depend on the covering fraction and temperature of the spot. A highly variable warp at the inner edge of the disk will produce quasi-periodic fluctuations that will cause extinction if the system is viewed close to edge-on, but will appear as fluctuating disk emission if the system is viewed closer to face-on. By quantifying the size, color (Section 4.1), and timescale (Section 4.2) of the fluctuations, we can add to our understanding of the underlying physical source of the variability (Section 5).

4.1. Color Variations

To begin to understand the source of the variability, we look for changes over time in the [3.6]–[4.5] color. To quantify the change in color, we measure the slope of the correlation between the [3.6] and [4.5] photometry, which translates into a direct measure of $\Delta[4.5]/\Delta[3.6]$ ($\Delta[3.6] = [3.6] - [3.6]$, $\Delta[4.5] = [4.5] - [4.5]$), and in turn a measure of the change in [3.6]–[4.5] averaged over the observing window. Previous studies (e.g., Poppenhaeger et al. 2015) have utilized color–magnitude diagrams, such as [3.6] versus [3.6]–[4.5], which contain the same information but are slightly biased by the correlated errors between the two axes. In our diagnostic, $\Delta[4.5]/\Delta[3.6] = 1$ indicates no change in color, $\Delta[4.5]/\Delta[3.6] > 1$ indicates a “blueing” (the source gets bluer as it gets fainter, or similarly, redder as it gets brighter), and $\Delta[4.5]/\Delta[3.6] < 1$ indicates a reddening (the source gets redder as it gets fainter, or similarly, bluer as it gets brighter). We measure the slope using the Python orthogonal distance regression method, which accounts for uncertainties in both axes, with results for those stars with substantial [3.6] and [4.5] overlap ($N_{\text{pair}} > 20$) listed in Table 4 and shown in Figures 6 and 7.

The majority of the YSOs are consistent with having no significant change in color. Given our typical uncertainties, this corresponds to $0.9 < \Delta[4.5]/\Delta[3.6] < 1.1$, or a change in [3.5]–[4.5] smaller than 0.05 mag for every half magnitude change in [3.6]. We do find four sources (533, 691, 720, and 1504; Figure 8) that become significantly redder as they get fainter ($\Delta[4.5]/\Delta[3.6] < 1$) and two sources (360 and 557; Figure 9) that become significantly bluer as they become fainter ($\Delta[4.5]/\Delta[3.6] > 1$). For these sources, the [3.6]–[4.5] color varies by 0.06–0.3 mag for every half-magnitude change in [3.6] magnitude. None of these color variations are large enough to change the evolutionary stage classification. Rebull et al. (2014) find such events to be very rare, occurring in $<0.02\%$ of infrared sources, although some cases have been found (Rice et al. 2012).

By measuring $\Delta[4.5]/\Delta[3.6]$, we are tracing the average change in color over the entire 200-day observing window. Multiple processes that produce opposite effects on the

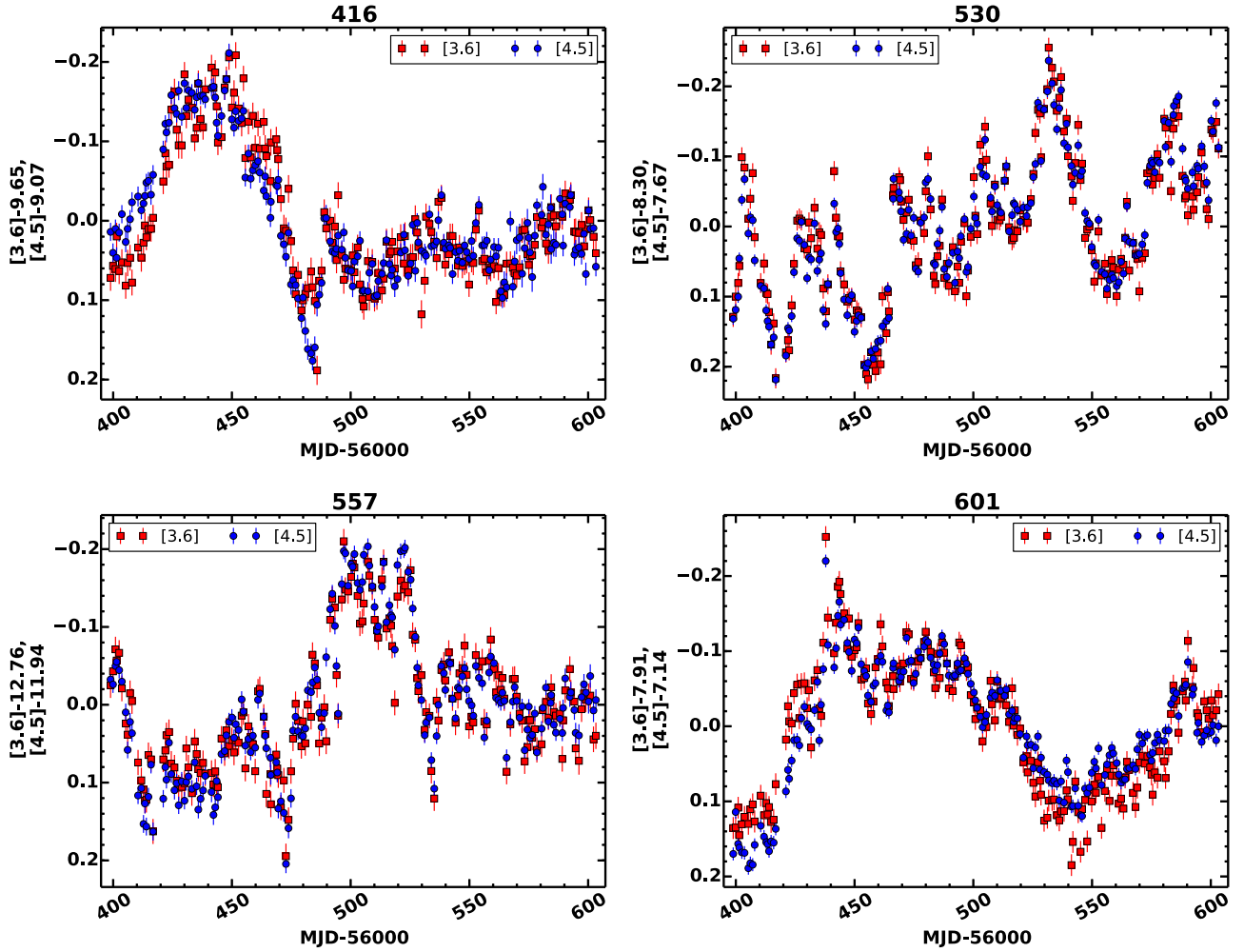


Figure 3. Infrared light curves for select cluster members. [3.6] data are marked with red squares, while [4.5] photometry is shown with blue circles. We see a wide variety of light curve shapes, with timescales covering the entire 200 day observing window. Light curves for all the detected cluster members are included in the figure set.

(The complete figure set (32 images) is available.)

color can operate simultaneously, effectively canceling each other out in the long term, while still producing short-term fluctuations in color. We see evidence for this in some of the light curves that show no average change in color (Figure 10), as well as the distribution of $\Delta[4.5]/\Delta[3.6]$ (Figure 7). Star 601 shows a long-term trend where it gets redder over the course of the observing window, before turning bluer over the last 40 days. Star 530 oscillates in color, with the color light curve tending to become bluer during outbursts, although not consistently and strongly enough to produce a significant signal in $\Delta[4.5]/\Delta[3.6]$. Star 416 gets significantly bluer during the large initial outburst, but has a relatively constant color afterward, while star 623 has a much shallower slope in $\Delta[4.5]/\Delta[3.6]$ when it is fainter. The structure in the light curves suggests that there may be a timescale dependence to the color variations, which we examine in more detail in Section 4.2.

Since the [3.6] and [4.6] flux is a mix of stellar and dust emission and stellar emission is hotter than the dust emission, changes to one or the other will have distinct effects on the observed color. We consider the variations in [3.6] and [4.5] for three scenarios: (1) hot/cold spots, (2) extinction, and (3) changes in the dust emission strength. The hot and cold spots

are modeled as $T_{\text{spot}} = 8000$ and 2000 K spots covering a fixed fraction of a star with an effective temperature representative of the median of the cluster (3500 K). With covering fractions of 5% and 30% for the hot and cold spot, we find $\Delta[3.6] = 0.16$ and 0.12 and $\Delta[4.5]/\Delta[3.6] = 1.1$ and 0.9 , respectively. A dust cloud with a depth of $A_K = 1$ creates $\Delta[3.6] = 0.6$ with a $\Delta[4.5]/\Delta[3.6] = 0.84$ based on the extinction law of Flaherty et al. (2007) and $\Delta[4.5]/\Delta[3.6]$ closer to 1 if the grains within the disk are larger than those in giant molecular clouds. To model variable dust emission, we consider a simple model with a $T_{\text{eff}} = 3500$ K blackbody representing the stellar emission underneath a $T_{\text{dust}} = 1500$ K blackbody with varying strength. This model is meant to mimic a system in which the stellar contribution to the [3.6] and [4.5] emission is constant while the contribution from the disk itself changes with time, possibly due to changes in the emitting area (e.g., scale height) of the dust. This model produces fluctuations of a few tenths of a magnitude with $\Delta[4.5]/\Delta[3.6] = 1.25$, with slight variations in this slope expected for stars of different T_{eff} and for different fiducial dust strengths.

Comparing the predictions from these phenomenological models to the data (Table 4, Figure 6), we find that fluctuations

Table 2
Infrared Variability

ID	[3.6]			[4.5]			N_{pair}	Stetson
	N_{epochs}	χ^2_{ν}	Δmag	N_{epochs}	χ^2_{ν}	Δmag		
75	121	23.6	0.22	6	30.7	0.13	0	...
100	91	1.8	0.07	26	1.7	0.06	0	...
239	185	1.5	0.05	73	1.6	0.03	58	0.01
299	86	2.0	0.06	71	1.4	0.04	0	...
330	200	22.9	0.19	111	56.1	0.20	111	5.1
360	200	6.6	0.10	122	25.7	0.12	122	2.3
383	47	4.1	0.41	49	44.9	1.05	31	0.4
402	0	25	5.6	0.15	0	...
403	188	36.2	0.21	137	61.2	0.18	125	4.3
416	200	25.1	0.21	200	45.4	0.22	200	4.1
439	117	214	0.53	114	566	0.54	59	15.0
530	200	46.9	0.26	200	129.1	0.26	200	6.8
533	126	43.8	0.27	179	147.7	0.27	105	5.6
557	200	25.5	0.23	200	67.9	0.27	200	4.8
593	92	1.5	0.04	150	1.1	0.03	42	0.06
601	200	36.5	0.22	200	88.6	0.21	200	5.9
602	91	6.0	0.08	153	30.9	0.12	44	1.5
623	199	7.7	0.16	200	18.3	0.17	199	1.9
691	88	129	0.44	200	207	0.32	88	10.5
720	62	26.0	0.19	197	61.1	0.16	59	4.7
791	79	7.0	0.10	20	5.7	0.06	0	...
793	158	11.4	0.14	94	16.6	0.11	52	2.1
966	90	1.3	0.05	155	1.2	0.04	45	-0.04
1034	56	43.2	0.25	188	256	0.37	44	5.8
1103	2	...	0.04	148	1.9	0.04	0	...
1504	55	18.0	0.19	196	50.0	0.16	51	3.1
2712	102	1.9	0.03	12	3.1	0.02	0	...
4342	87	1.3	0.09	2	...	0.04	0	...
5073	76	3.4	0.06	0	0	...
6555	0	118	1.4	0.03	0	...
8665	0	100	1.8	0.03	0	...
14260	0	39	2.1	0.05	0	...

Note. Infrared variability statistics for our sample. Included for each band are the number of epochs at which the YSO was detected with $\sigma < 0.1$ (N_{epochs}), the reduced chi-squared (χ^2_{ν} , with $\chi^2_{\nu} > 3$ indicating significant variability), and the difference between the magnitudes at the 10th and 90th percentiles. Also listed is the number of epochs with simultaneous [3.6] and [4.5] data (N_{pair}) and the Stetson index for those stars with $N_{\text{pair}} > 0$ ($S > 0.45$ indicates significant variability).

Table 3
Star-forming Region Comparison

Region	Variable Fraction	Δmag	Reference
Cha I	0.80	0.05–0.3	This work
IRAS:20050+2720	0.70	0.17	1
NGC 1333	0.62	~0.1	2
ONC	0.70	~0.2	3
L1688	0.85	0.1–0.26	4
GGD 12–15	0.70	~0.15	5
IC 348	0.60	~0.1	6
NGC 2264	~0.90	0.1–0.3	7

Note. Fraction of YSOs with an infrared excess that are variable in the infrared, as measured by *Spitzer*, and the typical range in $\Delta[3.6]$, $\Delta[4.5]$ as reported by these studies.

References. (1) Poppenhaeger et al. 2015; (2) Rebull et al. 2015; (3) Morales-Calderón et al. 2011; (4) Günther et al. 2014; (5) Wolk et al. 2015; (6) Flaherty et al. 2013; (7) Cody et al. 2014.

from hot/cold spots are inconsistent with the large observed fluctuations, and that the data are more consistent with either extinction or disk emission fluctuations. Dust emission

fluctuations are more consistent with the two sources that show “blueing” (Figure 9: stars 330 and 557), both of which exhibit Class II SED shapes. Extinction is most consistent with those sources that show reddening of their infrared colors (Figure 8: stars 533, 691, 720, and 1504). Of these sources, 720 and 1504 have Class II SED shapes, while 533 and 691 are more consistent with Class I objects. We note that $\Delta[4.5]/\Delta[3.6] < 1$ can be equivalently interpreted as meaning that the system becomes redder as it becomes fainter, or that it becomes bluer as it becomes brighter. The former interpretation can be explained by dust extinction, while the latter is more characteristic of a large increase in the hot accretion emission. Star 533, discussed in more detail below, may be better explained by an accretion outburst rather than obscuration by dust.

Previous studies have found similar results in other clusters. Poppenhaeger et al. (2015) find that color changes in the *Spitzer* bands of the YSOs in IRAS:250050+2720 are consistent with a mix of extinction and disk variability, with spots more prevalent among sources with heavily depleted dust emission. Wolk et al. (2015) also find that extinction and disk emission changes are most consistent with the *Spitzer* variability in the cluster GGD 12–15. Near-infrared studies of

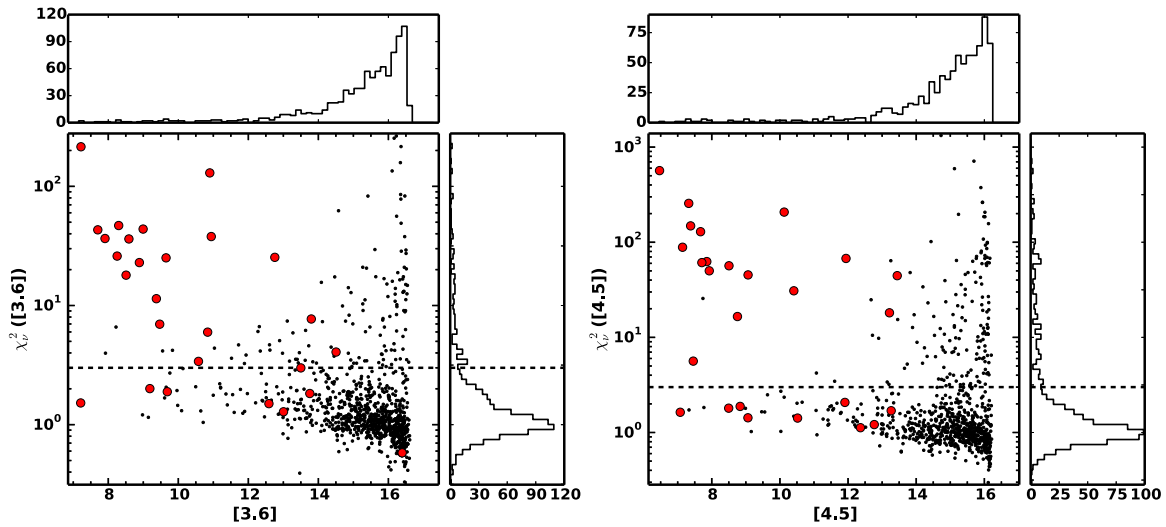


Figure 4. Distribution of reduced chi-squared values and mean magnitudes for [3.6] (left) and [4.5] (right). All detected sources with more than 20 epochs in a particular band, predominately foreground and background stars, are shown with black dots, while known cluster members are marked by large red circles. The horizontal dashed line indicates a reduced chi-squared of three; points above this line are considered significantly variable.

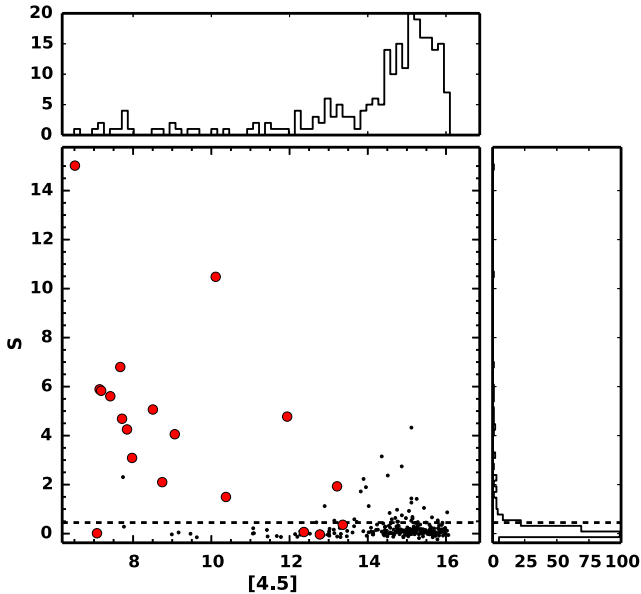


Figure 5. Stetson index as a function of [4.5] magnitude. All detected sources, composed mostly of background and foreground stars, with more than 20 simultaneous [3.6] and [4.5] detections are shown with black dots, while known cluster members are marked with large red circles. The horizontal dashed line indicates a Stetson index of 0.45, above which sources are included as variable.

Orion have also found similar results (Carpenter et al. 2001; Parks et al. 2014), with a larger role for spots due to the shorter-wavelength near-infrared bands being more sensitive to stellar emission.

4.2. Timescale of the Variability

Another property that can help to determine the nature of the variability is its timescale. Processes associated with the stellar surface, such as heating of the disk by variable hot spots (e.g., Herbst et al. 1994; Nagel et al. 2015), will operate on a timescale similar to the stellar rotation period, which is typically 1–15 days (Rebull et al. 2004, 2006; Cieza &

Baliber 2006; Cody & Hillenbrand 2010). The timescales of “dippers,” in which the flux briefly decreases on quasi-periodic timescales of days, have been used to constrain the location of the obscuring material too close to the star (McGinnis et al. 2015; Stauffer et al. 2015). Processes originating in the disk will operate on the local dynamical timescales, which can range from weeks to years. Periodic fluctuations indicate stable, long-lived effects, while aperiodic behavior indicates that the features responsible for the variability are quickly created and destroyed. When combined with the color information discussed above, the physical cause of the variability can be constrained. Here, we search for periodic fluctuations and also characterize the power spectrum of the aperiodic fluctuations that are seen among the majority of stars.

4.2.1. Periodicity

We look for periodic behavior using the NASA Exoplanet Archive Periodogram Service,⁹ which examines the light curves using the Lomb–Scargle periodogram (Scargle 1982), the box-fitting least-squares algorithm (Kovács et al. 2002), and the Plavchan algorithm (Plavchan et al. 2008). Each light curve has been smoothed by a 50-day moving average; long-term trends in the data will enhance the power at low frequencies, resulting in spurious period detections. We consider a star as periodic if one of the methods finds a peak with power >20 , which roughly corresponds to a false-alarm probability $<10^{-5}$; this period is recovered in the other methods and in both wavelengths. We also confirm the variability based on the presence of well-phased features at the measured period. This conservative set of criteria results in only five periodic stars (Table 5), for a periodic fraction of $16^{+17}_{-11}\%$ (5/32). Although the period search algorithms are sensitive to weaker variability than the χ^2_ν or Stetson index, no periodicity was detected in a source for which the χ^2_ν or Stetson index did not already indicate strong variability.

Two of the periodic stars (330 and 691) exhibit short periods ($P = 7.9$ days), with original and phased light curves for these

⁹ <http://exoplanetarchive.ipac.caltech.edu/cgi-bin/Pgram/nph-pgram>

Table 4
Color Changes

ID	N_{pair}	$\Delta[4.5]/\Delta[3.6]$
330	111	0.99 ± 0.03
360	122	1.61 ± 0.12
403	125	0.92 ± 0.03
416	200	1.01 ± 0.03
439	59	0.97 ± 0.02
530	200	1.01 ± 0.02
533	105	0.85 ± 0.04
557	200	1.13 ± 0.02
601	200	0.96 ± 0.03
602	44	0.96 ± 0.10
623	199	1.15 ± 0.06
691	88	0.75 ± 0.01
720	59	0.81 ± 0.03
793	52	1.02 ± 0.08
1034	44	1.13 ± 0.05
1504	51	0.80 ± 0.04
Hot spot	...	1.1
Cold spot	...	0.9
Extinction	...	0.84
Disk changes	...	1.25

two sources shown in Figure 11. Both of these sources have M1–M2 spectral types, with 330 displaying a Class II SED shape, while 691 has a Class I SED shape. To test whether the similarity in the periods of these two systems is an artifact of, e.g., the time sampling or is simply a coincidence, we repeat our period search on randomly shuffled versions of the light curves of stars 330 and 691. We do not find any significant (false-alarm probability <0.05) peaks at $P = 7.9$ days, or any other period, in these shuffled light curves. Similarly, we examine the light curves of nonvariable noncluster members and again find no significant peaks near 7.9 days. This indicates that the similarity between the periods of these two sources is a coincidence.

While the stellar rotation period has not been directly measured for these two stars, the observed period is similar to what has been measured in YSOs of similar ages (Rebull et al. 2004). In the optical, periodic variability is often associated with the rotation of cold spots across the visible stellar surface (Herbst et al. 1994), although as discussed above, the size and color of the fluctuations within these objects are not consistent with a spot interpretation. Instead, we may be seeing periodic obscuration of the stellar surface by a large warp at a location in the disk close to the corotation radius, a scenario that is discussed in more detail in Section 5.

The other three periodic sources (439, 530, and 533) have timescales (32, 35, and 36 days, respectively) that are much longer than expected from stellar rotation, suggesting that the variability is not associated with motion close to the stellar surface. All three show strong fluctuations ($\Delta[3.6] = 0.53, 0.26, 0.27$, respectively) and have a strong infrared excess; 439 and 530 are Class II sources, while 533 is a Class I source. The small number of sources prevents any strong interpretation, but we note that Rebull et al. (2014) also found an infrared excess to be common among stars with longer periods. Light curves for our three long-period sources are shown in Figure 12. For stars 439 and 533 there is a consistent shape among the different cycles, while the phased light curve of star 530 highlights the fact that the size of the fluctuations and possibly

their period vary from one cycle to the next. The periods correspond to Keplerian orbits at distances of ~ 0.2 au. Previous surveys of near-infrared variability have found stars with periods over 100 days (Plavchan et al. 2008; Wolk et al. 2013; Parks et al. 2014), indicating that long-period behavior is not uncommon among YSOs.

4.2.2. Understanding the Timescale of Aperiodic Variability

The majority of our cluster members are aperiodic, with fluctuations operating on a range of timescales. Even star 530, which shows significant periodicity, has a long-term trend underlying the periodic behavior. The stochastic nature of much of the variability means that many cycles must be observed before the average size of the fluctuations can be accurately measured. Further complicating this analysis is that statistical tools designed to quantify the size of the fluctuations as a function of frequency, such as the structure function (Hawkins 2002; de Vries et al. 2003) or Lomb–Scargle periodogram (Scargle 1982), suffer from biases due to the finite sampling and limited observing window (Emmanoulopoulos et al. 2010; Findeisen et al. 2015). To accurately quantify the strength of the fluctuations as a function of frequency, we utilize recent work in understanding AGN variability as laid out in Kelly et al. (2009) and Kelly et al. (2014) and contained in the CARMA_PACK software package.¹⁰ In short, this code uses a continuous-time autoregressive moving average (CARMA) stochastic model to fit the light curve. The power spectrum is then derived analytically from the parameters of the light-curve model, avoiding systematic distortions of the power-spectrum shape by the finite sampling of the observed light curves. The Bayesian framework for the model fitting includes an accounting of the uncertainties in the data, which is translated into posterior distributions for the model parameters and statistical uncertainties in the shape of the power spectrum. With statistically robust estimates of the power spectrum that are unbiased by the observing cadence, we can begin to characterize the relative strength of the stochastic fluctuations on different timescales and use this information to better understand the source of the variability.

In Figure 13 we highlight power spectral density curves that display some of the common behaviors seen among our sample. The bands in these figures represent the 95% confidence interval on the shape of the power spectrum, while the horizontal lines represent the noise level of the power spectrum. We find that almost every source exhibits an increase in power toward low frequencies that is roughly consistent with $P(f) \propto f^{-2}$. The only source whose power spectrum is not dominated by a power-law decline is 691. In this case the light curve is deterministic and not intrinsically stochastic, thus violating one of the assumptions of the CARMA model, and we exclude it from our analysis in the context of the CARMA model. The power-law shape seen in the power spectral density indicates that the fluctuations are not dominated by day- to week-long timescales, but instead exhibit behavior covering a large range of timescales. Within each object, as the timescale increases, the size of the fluctuations increases. Previous *Spitzer* surveys predominately sample frequencies down to 0.03 day^{-1} , while our data are able to extend down to 0.005 day^{-1} . The 200-day span of our survey prevents us

¹⁰ https://github.com/brandonckelly/carma_pack

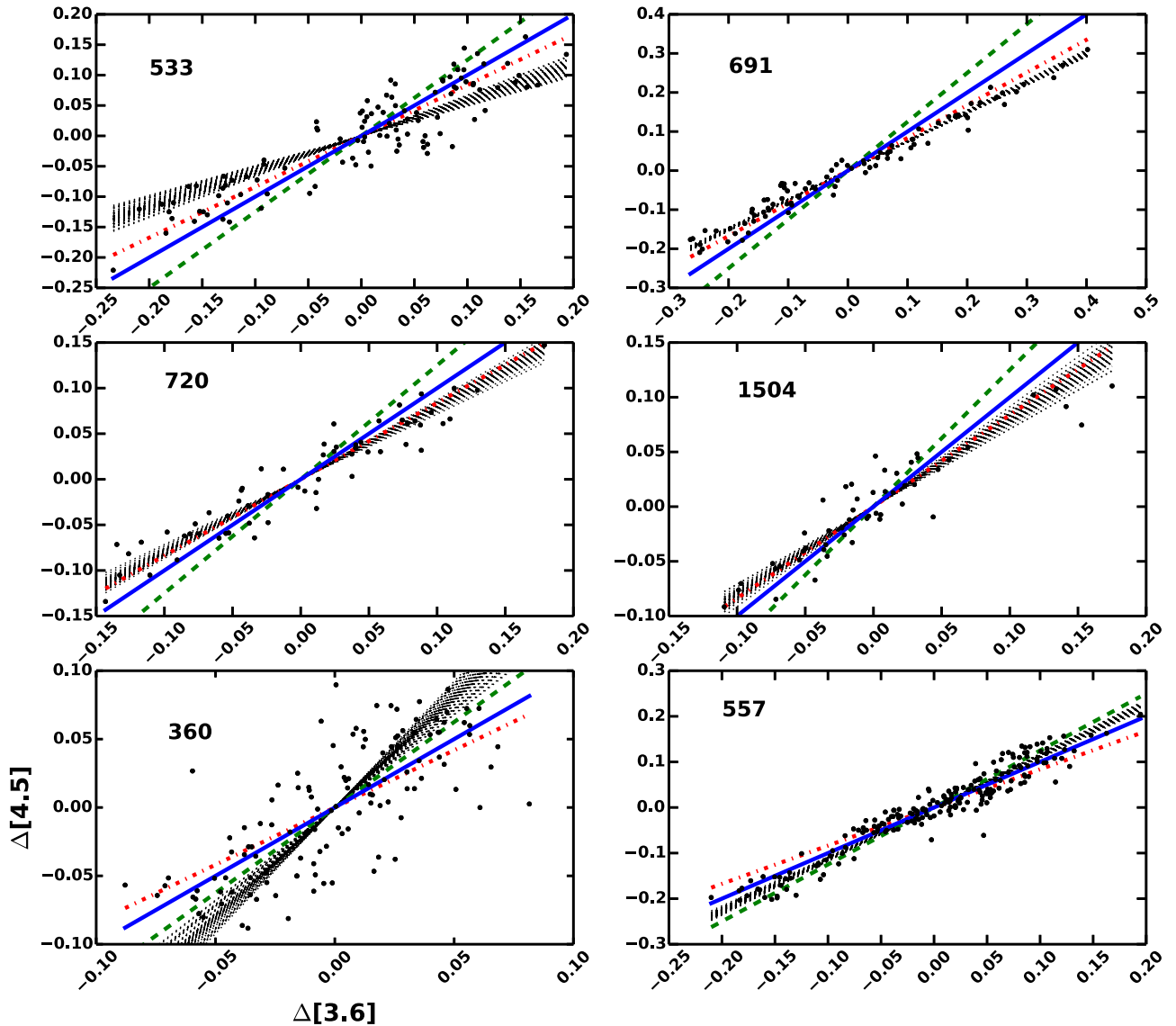


Figure 6. Change in the [3.6] and [4.5] magnitude for the six sources with significant color variations. The blue solid line shows no change in color, the red dotted line shows extinction by $A_K = 1$, and the green dashed line shows a change in dust emission. The measured slope, along with its uncertainty, is indicated by the distribution of dashed lines. The first four systems (533, 691, 720, 1504) exhibit reddening, while the last two systems (360, 557) experience bluing.

from determining whether the power-law shape extends to lower frequencies, although there is evidence for fluctuations over years, as discussed below. The combination of high cadence and long-baseline observations within our survey allows us to derive the smooth connection between daily and months-long infrared fluctuations as seen in the approximately power-law shape of the power spectrum.

The presence of long-timescale fluctuations is consistent with recent *Spitzer* and ground-based near-infrared surveys, although with less dense time coverage. Rebull et al. (2014) identify a handful of objects with variations between *Spitzer* observations separated by 6–7 yr. Interestingly, they find that these long-term variables are more common among clusters with a higher fraction of Class I protostars and hence are likely younger. Parks et al. (2014) observe ρ Oph over the course of 2.5 yr and find long-term variations in 31% of the sample, with timescales ranging from 64 to 790 days, with 68% of the variable systems showing a long-term trend over the entire 2.5 yr period. Wolk et al. (2013) in their near-infrared study of Cyg OB7 also find variability on timescales of years, consistent with

the previous surveys. In their study of four young clusters, Scholz (2012) find that the frequency of highly variable objects ($\Delta m > 0.5$) increases with the length of the time window (from days to years). Megeath et al. (2012) find variability to be common in *Spitzer* observations of Orion that cover a 6-month baseline. In near-infrared observations spanning almost 900 days, Rice et al. (2015) find variability to be common, with fluctuations consistent with accretion/disk variability having a longer timescale than those associated with variable obscuration. These results indicate that even our 200-day time coverage may not span the entire range of the variability, as discussed in more detail below.

On top of the power-law behavior, we also occasionally find sharp peaks at high frequencies. This is best exemplified in star 623, where this peak is detected at the $>3\sigma$ level, although 1σ – 2σ peaks are seen in other sources. These features do show up in sources for which the Lomb–Scargle periodogram indicates periodic behavior (e.g., 330), but, as in the case of star 623 (discussed in more detail in the Appendix), this feature is not always picked up in our period search. This may be due to the

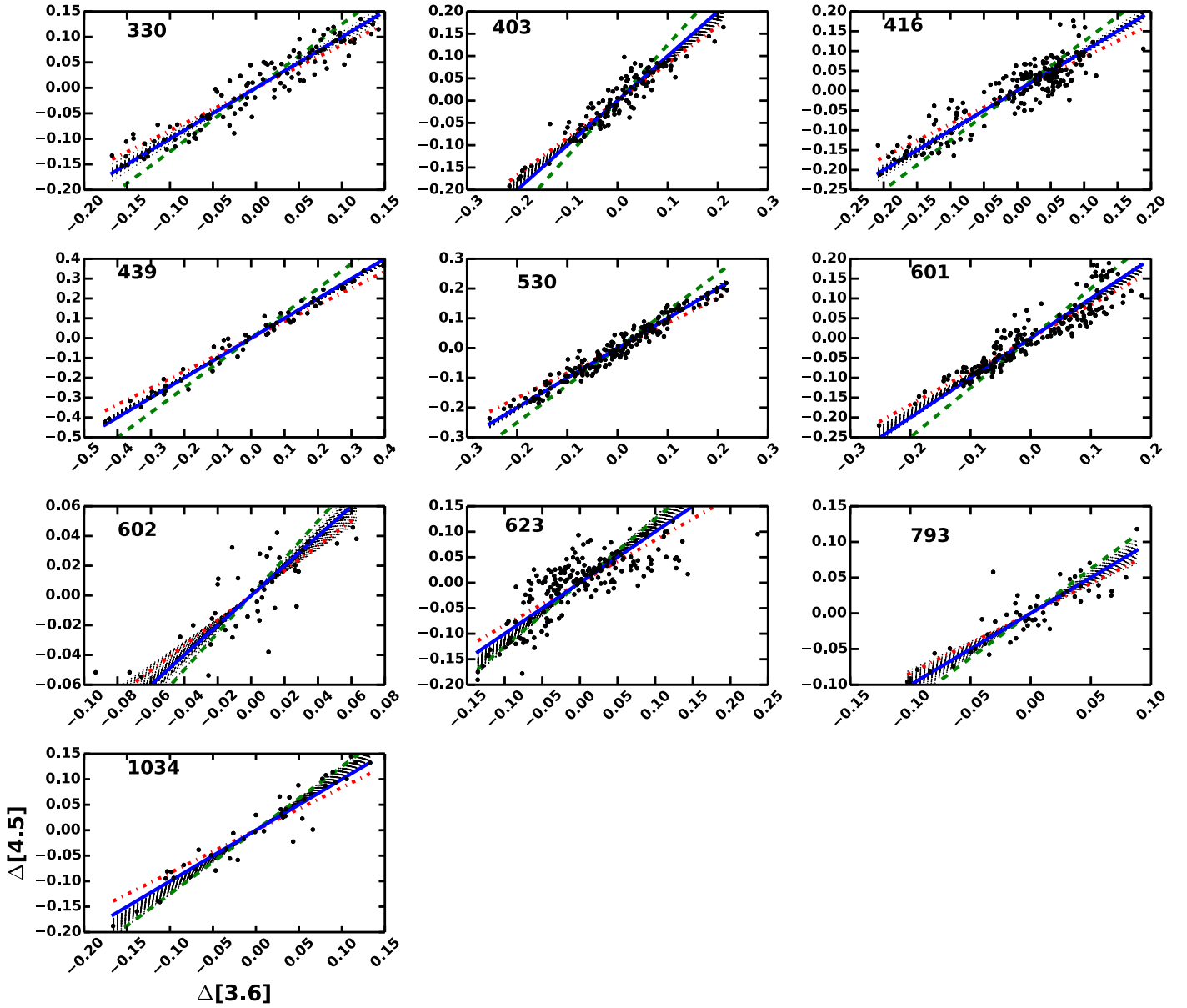


Figure 7. Change in the [3.6] and [4.5] magnitude for the 10 sources with substantial overlap in both bands but no significant average color variations. Lines and points are as in Figure 6. Even when the color does not vary on average, there are points that follow the extinction or disk fluctuation model predictions, indicating that a mix of different processes may be operating within these systems.

stochastic nature of the periodic behavior. The Lomb–Scargle periodogram assumes that the amplitude and frequency of any periodic behavior are constant throughout the light curve, while the CARMA model is designed for more stochastic behavior. Additional data at a higher observing cadence will help to confirm many of these features.

4.2.3. Very Long Timescale Variability

While our survey only covered 200 days, we can use these data in combination with previous infrared surveys to help characterize the very long term variability. Previous studies have found year-to-year fluctuations (Parks et al. 2014; Rebull et al. 2014; Wolk et al. 2015), suggesting that infrared variability is not limited to the timescales studied here. *Spitzer* was used to survey the Chameleon star-forming region in 2004 and 2005 (Luhman et al. 2008), covering our field of view, at a

similar depth, allowing a direct comparison of measured photometry. There are 16 sources within our sample for which either the [3.6] or [4.5] flux differs significantly between the previous measurements and our survey (Table 6), suggesting fluctuations on decade-long timescales. The prior photometry differs by 0.1–0.5 mag from the average of our observations, which corresponds to fluctuations 3–5 times larger than we observe. These larger fluctuations on longer timescales are roughly consistent with an extension of the $P(f) \propto f^{-2}$ seen in our derived power spectral density functions, which would predict fluctuations ~ 4 times larger on a 9 yr timescale than on a 200-day timescale, although more work is needed to confirm this behavior.

Year-long fluctuations can also be probed by comparing data taken by the *Wide-field Infrared Survey Explorer* (WISE; Wright et al. 2010) in the cryo and post-cryo (NEOWISE; Mainzer et al. 2011) campaigns. *WISE* surveyed the entire sky

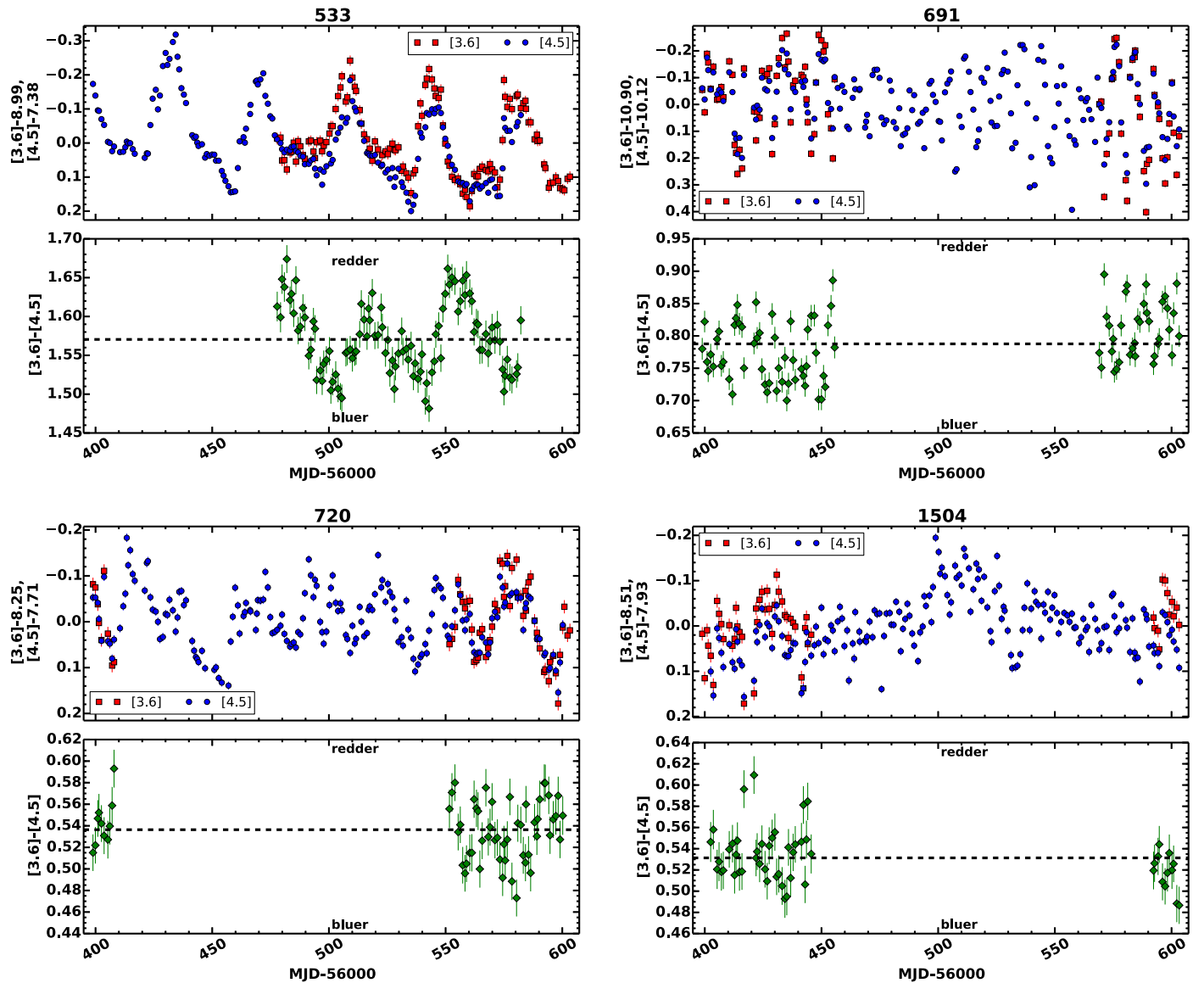


Figure 8. Light curves of stars that get significantly redder as they get fainter ($\Delta[4.5]/\Delta[3.6] < 1$). This reddening behavior may be a sign of extinction by small dust grains.

in four infrared bands, of which the shortest two have central wavelengths of 3.4 and 4.6 μm , similar to that of *Spitzer*. During its cryogenic campaign, *WISE* observed Cha I in 2010 February and August, while the post-cryo NEOWISE campaign observed Cha I over four blocks in February and August of 2014 and 2015, providing a 5 yr total baseline. Of the 19 sources in our sample detected in both bands in both campaigns, two show a substantial change in flux between the *WISE* and NEOWISE campaigns, of a few tenths of a magnitude. The smaller number of sources with long-term fluctuations detected by *WISE* as opposed to with *Spitzer* is likely not due to sensitivity (both the *WISE* and *Spitzer* photometry have uncertainties of 0.01–0.02 mag), but because the NEOWISE data cover a year-long span and likely already capture much of the slow fluctuations.

Another form of long-term variability is when the size of the fluctuations changes over time. *WISE* can help to address this since it observed Cha I during its cryogenic phase in two short blocks, one covering 2010 February 14–16 and the other covering 2010 August 12–17, with a total time coverage similar

to our survey. By looking for sources that are variable in the *WISE* data but not in our survey, or vice versa, we can begin to characterize the frequency of large changes in the amplitude of infrared variability. Of the 11 nonvariable sources in our sample, one (#2712) shows significant variability (~ 0.1 mag) in the *WISE* data that, if still ongoing, would have been detectable in our survey. The majority of the *Spitzer* variable sources are also variable in the *WISE* data, with the exception of 602, 523, 1034, and 1504. While the fluctuations in 602 are small (~ 0.05) and may not have been detectable with *WISE*, the fluctuations in the other three stars are ~ 0.1 mag and should have been detectable with *WISE*. Similarly, comparing the *WISE* and NEOWISE observations, there are seven sources that show evidence of variability in NEOWISE but are not detected as variable in the cryogenic *WISE* campaign. This suggests that some disks do change the strength of their variability on timescales of years. As with the slow modulations seen between the *Spitzer* epochs, this indicates that there are further long-term changes in circumstellar disks that are not fully probed by our survey. Whether or not these long-term

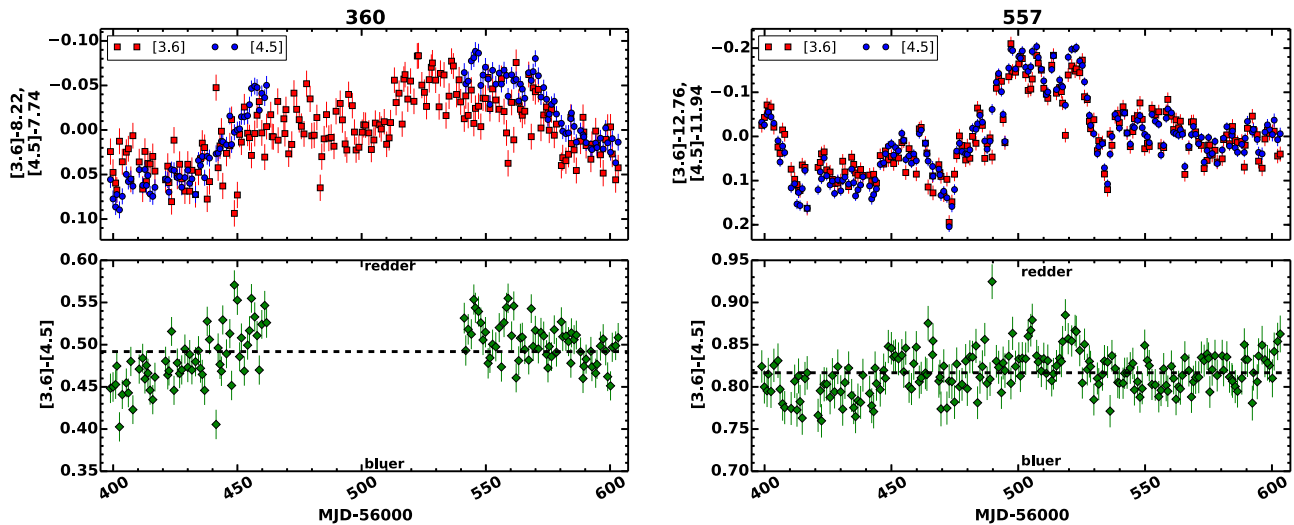


Figure 9. Light curves of stars that get significantly bluer as they get fainter ($\Delta[4.5]/\Delta[3.6] > 1$). This behavior may be a sign of variable dust emission.

fluctuations are physically related to the months-long variability, or a sign of distinct processes, is discussed in more detail below.

4.2.4. Color Variations with Time

So far in analyzing the timescale of the fluctuations we have focused on changes in the [3.6] and [4.5] individually, but as noted in Section 4.1, the [3.6]–[4.5] color is not constant in all of our targets. The behavior of the color with time may also probe the physical cause of the variability (i.e., stable spots cause periodic variations in both flux and color).

Inspecting the light curves of the stars with significant color variations (Figures 8, 9) reveals additional trends. In star 1504 there are distinct reddening events at the moments when the [3.6] and [4.5] flux drops, while in star 533 the color shows the same oscillations as the total flux, with the bluest color at the beginning of the outburst. Even among the stars that show no overall change in color, there is structure in their color light curve (Figure 10).

Applying the CARMA_PACK tool to the [3.6]–[4.5] light curves, we find that the power spectral density has a roughly power-law behavior (Figure 14), similar to the [3.6] and [4.5] magnitudes. Only star 330 has color fluctuations consistent with the noise at all timescales. Significant fluctuations are only detected on timescales $\gtrsim 50$ days due to the small size of the variability relative to the noise, making it difficult to search for the narrow high-frequency features seen in the [3.6] and [4.5] power spectral densities. Despite these limitations, it appears that the change in color increases with timescale. This is seen even among sources that do not have a significant average change in color (stars 360, 416, 530, 601, and 623). This can occur if the direction of the change in color, which is not captured by the CARMA model, varies with timescale (e.g., extinction dominates on short timescales while disk changes dominate on longer timescales).

The derived power spectral densities only apply to timescales up to 200 days, but we can constrain slower effects by comparing our measured color with that of Luhman et al. (2008). We find that 11 stars (100, 330, 530, 533, 602, 623, 691, 966, 1103, 2712, and 4342) show a significant variation of color (0.1–0.6 mag) over the roughly decade between these observations. Half of these very long timescale variations are

consistent with disk fluctuations, while half are consistent with extinction. In none of these sources does the color change enough to affect the SED classification. Of these 11 sources, four (530, 533, 602, and 623) show an increasing color power spectrum in our data, one (330) has a color power spectrum below the noise, and for the remaining six (100, 691, 966, 1103, 2712, and 4342) we do not have enough data to constrain the color variations in our survey. The presence of color variations over such long timescales is consistent with increased color fluctuations with time, as was seen with the power spectral density curves.

5. DISCUSSION

We find that long-timescale variability (20–200 days) is common among YSOs and the color changes observed in our sample are consistent with a mix of extinction and disk emission fluctuations. This behavior is an extension of the short-timescale variability seen in previous surveys and may continue to even longer timescales. Here we consider a handful of possible models for infrared variability that can be constrained by our observations.

Starspots: optical variability is often associated with the rotation of hot or cold spots across the stellar surface (Herbst et al. 1994). Spots can be seen in the mid-infrared in systems with very little dust emission (Poppenhaeger et al. 2015), as well as in the near-infrared (Carpenter et al. 2001; Parks et al. 2014; Wolk et al. 2015), where the contribution to the observed flux from the dust is weaker and the stellar flux is stronger. Since the spots are affixed to the stellar surface, they generate periodic signatures in the light curve at the stellar rotation period. This periodicity is more often seen with cold spots, which tend to be long-lived, than with hot spots, which tend to vary substantially in size from one period to the next (Herbst et al. 1994). We do find two sources with stable periods consistent with stellar rotation ($P = 7.9$ days for stars 330 and 691), but the size of the observed fluctuations ($\Delta[3.6] = 0.19, 0.44$) is much larger than expected for spots ($\Delta[3.6] < 0.15$). Also, both sources have a strong infrared excess, and 330 is a Class II source while 691 is a Class I source, making the spot explanation less likely.

Spots are more likely an explanation for those sources with little to no infrared excess. While Class I and II sources are the

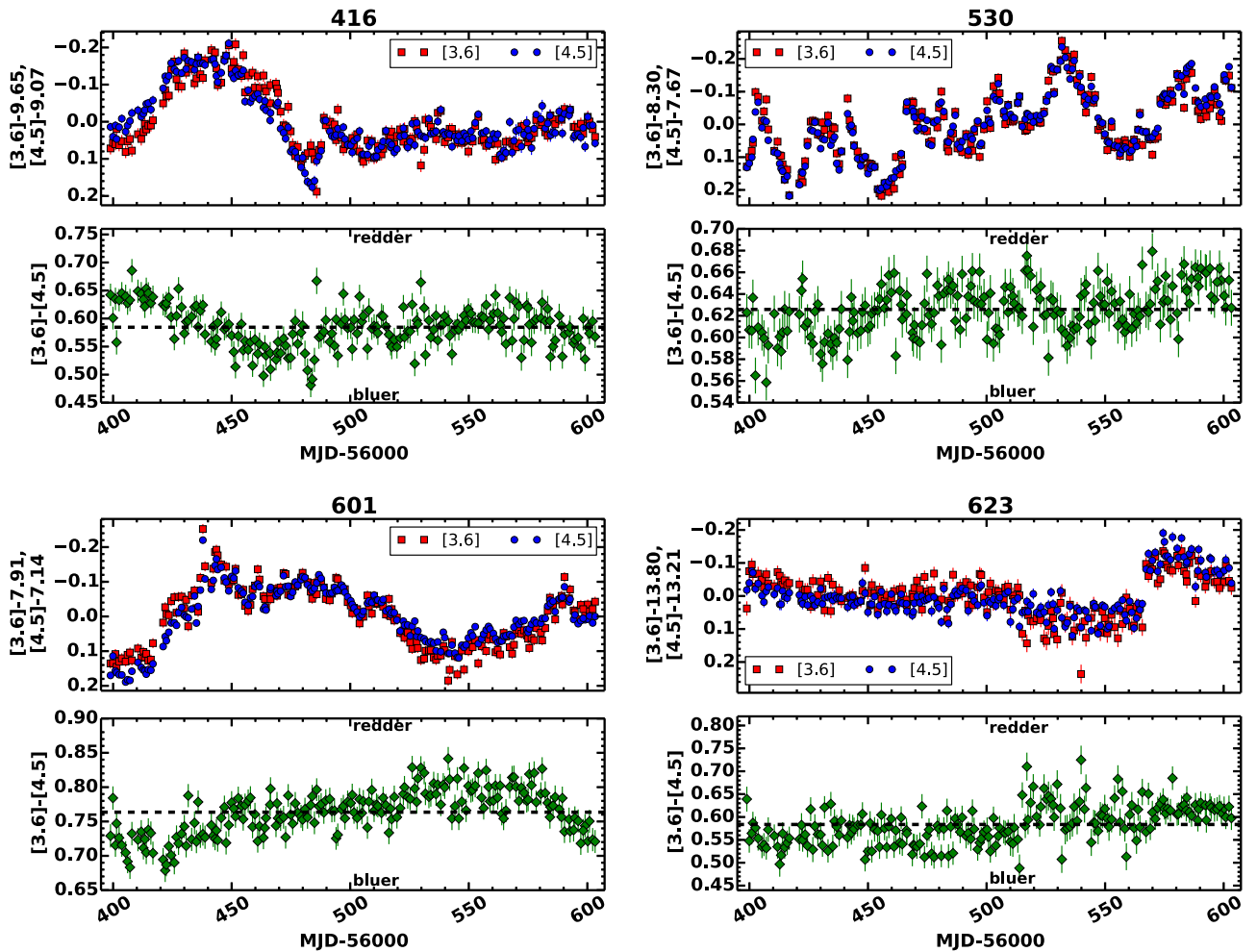


Figure 10. Light curves of stars for which the average color does not vary, but the color varies on short timescales within the light curve. A mix of multiple processes (extinction, disk fluctuations, etc.) may cancel each other out, producing effectively zero change in overall color over the course of the entire observing window.

main focus of our survey, there are two variable Class III sources within our sample (2712 and 5073). In both cases the fluctuations are small ($\Delta\text{mag} \sim 0.03\text{--}0.06$) and consistent with that expected from cold spots. There is no strong evidence for periodicity in the light curves, although the fluctuations are at the edge of our detection limit, making any periodic signal difficult to detect.

Perturbation from a companion: some known tight binaries show strong variability due to changes in the accretion flow associated with the eccentric motion of the companion (Basri et al. 1997; Mathieu et al. 1997; Jensen et al. 2007). Wider binaries can experience periodic dimming as components of the binary pass behind a circumbinary disk, as is the case in KH 15D (e.g., Windemuth & Herbst 2014; Arulanantham et al. 2016). The 131-day-period WL 4 system (Plavchan et al. 2008) and the 93-day-period YLW 16A system (Plavchan et al. 2013) show similar dimming behavior, suggesting a similar origin for their variability. A companion misaligned with the disk can also drag material out of the midplane (Fragner & Nelson 2010), leading to periodic occultations of the primary star. Periodic variability has been used to infer the presence of a tight binary in sources in which the central objects cannot be directly observed (Muzerolle et al. 2013). The motion of the binary can result in stable periodic fluctuations on timescales extending from days to thousands of years, depending on the separation of the two stars. Previous near-infrared surveys have

found stars with up to 90-day periodic variations (Wolk et al. 2013; Parks et al. 2014), and binarity is known to be common among YSOs (e.g., Nguyen et al. 2012). While the majority of the observed sources in Cha I exhibit aperiodic behavior, a small handful (439, 530, 533) are periodic with timescales (~ 30 days) that are longer than typical stellar rotation periods, and are consistent with a companion, such as a massive planet or low-mass star, at a separation of ~ 0.2 au.

Star 533 exhibits outburst behavior reminiscent of that seen in LRL 54361, which is characterized by ~ 3 mag outbursts every 25 days (Muzerolle et al. 2013). More recently, Hodapp & Chini (2015) discovered another outbursting Class 0/I object in Orion with similar properties ($\Delta K = 2$ mag, $P = 30$ days). Such behavior can be explained by material being dragged inward from the circumbinary disk during apastron, which eventually causes a large outburst in accretion luminosity as it falls onto the stars during periastron. Star 533 had been noted as a possible FUOr outbursting star by Gramajo et al. (2014), with K -band outbursts of 2 mag. While the period of star 533 in our data ($P = 37$ days) is slightly longer and the size of the fluctuations (~ 0.4 mag) is smaller than for these other objects, all three are deeply embedded Class I objects with stable periods. Star 533 also gets bluer as it becomes brighter (Figure 8), similar to the behavior seen in LRL 54361, which is consistent with an enhanced contribution from high-temperature accretion luminosity during outbursts. In this

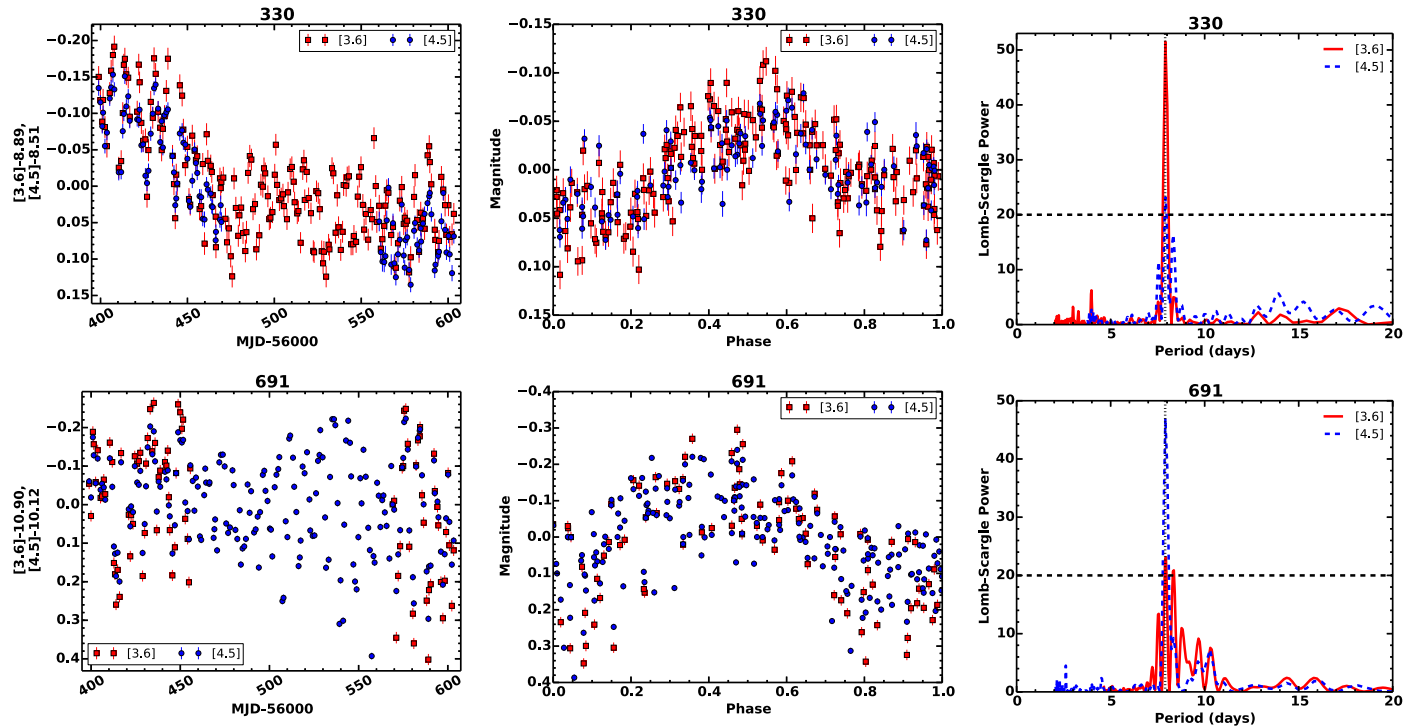


Figure 11. Original (left) and phased (middle) light curves, along with the Lomb–Scargle periodogram (right), for the two sources that show rapid ($P = 7.9$ days) periodic behavior. In the periodograms the horizontal line marks the boundary for a significant signal, while the vertical dotted line indicates a period of 7.9 days. The slow decrease in flux in star 330 has been removed to better highlight the rapid periodicity.

way, 533’s variability is consistent with the presence of an unseen, tight, eccentric binary driving periodic accretion bursts.

The source of the periodicity in stars 439 and 530 is less clear, but may still be connected with a binary. Star 439 exhibits a strongly sinusoidal pattern with a period of 33 days and is one of the strongest variables in the sample, with $\Delta[3.6], [4.5] = 0.53, 0.54$. Phase-folding the light curves reveals a dip in flux near its peak of ~ 0.2 mag (Figure 12), possibly associated with obscuration of the central source. Luhman et al. (2008) observe significant variability at $24\ \mu\text{m}$ with MIPS, with the $[24]$ magnitude varying from 1.46 ± 0.04 in 2004 to 1.80 ± 0.04 in 2005. It also has a high accretion rate; at $\dot{M} = 4.7 \times 10^{-8} M_{\odot} \text{ yr}^{-1}$ its accretion luminosity is $\sim 50\%$ of the stellar luminosity (Antoniucci et al. 2011). Star 530 exhibits an irregular sinusoidal pattern on top of a longer-term trend, with modest variations in flux ($\Delta[3.6], [4.5] = 0.26, 0.26$). It shows no significant average change in color, although there is evidence for small fluctuations in color that follow the sinusoidal pattern (Figure 10) and an increase in color fluctuations toward long timescales (Figure 14). This source was observed to be variable in *WISE* observations in 2010 (Table 6), suggesting that the fluctuations observed here are not a recent phenomenon. The phased light curve highlights the fact that the size of the fluctuations and possibly their period vary from one cycle to the next. While no other significant periods are detected consistently in both bands, they may still exist at a weak level.

While the presence of an unseen binary is difficult to constrain from the infrared variability alone, if all three of these systems were binaries, it would be consistent with the expected fraction of tight binaries. Nguyen et al. (2012), in their spectroscopic binary survey of Cha I with sensitivity to $\sim 0.1 M_{\odot}$ companions and periods less than 60 days, find that 7% of cluster members in Cha I are tight binaries, similar to surveys

of other clusters (Tobin et al. 2009; Reipurth et al. 2014; Kounkel et al. 2016). Further work is needed to confirm the binary nature of these three sources and its role in driving the infrared variability.

Heating by variable accretion: gas flows inward through the disk and along stellar magnetic fields lines, where it free-falls onto the stellar surface. This is a highly variable process, with emission-line measurements finding variations up to a factor of three on timescales of days (Nguyen et al. 2009; Costigan et al. 2014). Recent analysis of well-sampled optical light curves of YSOs in the NGC 2264 cluster finds that some of the optical variability can be explained by a mix of strong (Stauffer et al. 2014) and weak (Stauffer et al. 2016) accretion bursts. Shocks created as gas strikes the stellar surface are associated with high-temperature emission, and while this emission does not directly contribute much to the mid-infrared flux, it may heat the dust in the inner disk, leading to potentially observable infrared fluctuations. Large (orders of magnitude) outbursts in accretion certainly lead to variable infrared emission (Audard et al. 2014) and may apply in some cases here (e.g., star 533), but in this section we focus on the more modest fluctuations that occur more frequently among YSOs.

To affect the heating of the inner disk, the variable accretion luminosity must be substantial compared to the more stable stellar luminosity. Among the sources within our sample with measured accretion rates (Hartmann et al. 1998; Antoniucci et al. 2011; Robberto et al. 2012; Frasca et al. 2015; Manara et al. 2016), typical $L_{\text{acc}}/L_{*} \sim 0.1\text{--}0.4$, consistent with surveys of other low-mass star-forming regions (e.g., Antoniucci et al. 2014). Some variation is seen in the accretion rate as measured by different surveys, but part of this may be due to differences in methodologies for deriving the accretion rate rather than real fluctuations. Nagel et al. (2015) use detailed radiative transfer models of the inner disk and find that, starting with such modest

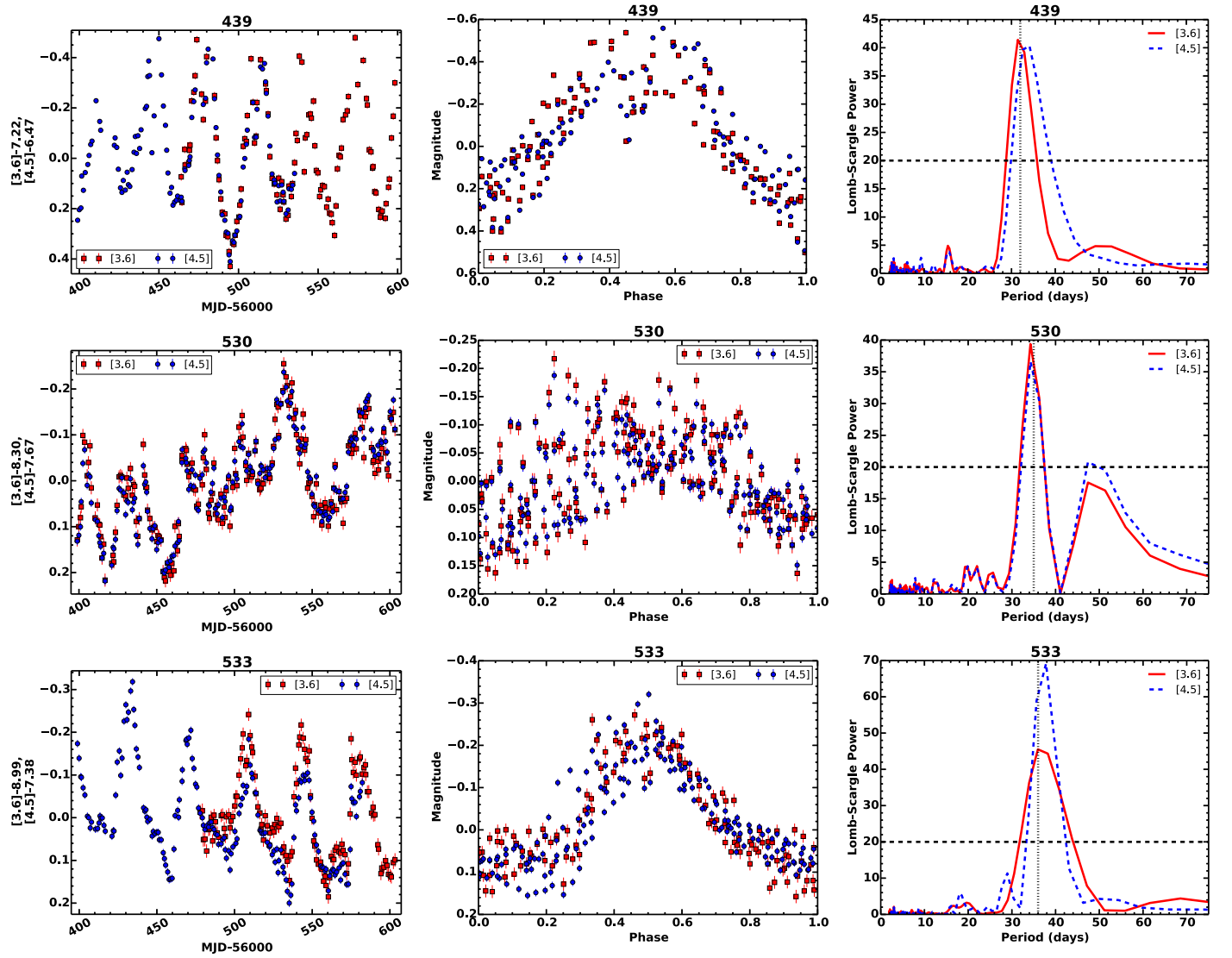


Figure 12. Original (left) and phased (middle) light curves, along with the Lomb–Scargle periodogram (right), for the three sources that show slow periodic behavior ($P = 32, 35$, and 36 days from top to bottom). In the periodograms the horizontal line marks the boundary for a significant signal and vertical dotted lines indicate the most significant period.

accretion luminosities, they can reach $\Delta[3.6] \sim 0.1\text{--}0.2$ with changes in accretion rate of 2–3 orders of magnitude. The required accretion rate variations are much larger than typically observed except in the most extreme cases, suggesting that variable heating is unlikely unless an asymmetric feature within the disk, such as a warp lined up with the accretion shock (Morales-Calderón et al. 2011), amplifies the effect.

Accretion variability also appears to operate on days- to week-long timescales (Costigan et al. 2014; Stauffer et al. 2016), corresponding to the dynamical timescale at such small distances from the star (Romanova et al. 2008). This suggests that variable accretion heating of the inner disk is most viable in systems with not only high accretion luminosities but also variability timescales on the order of days. Star 439 has the highest L_{acc}/L_* , but its stable period is inconsistent with the generally stochastic nature of variability associated with accretion variations (Herbst et al. 1994; Stauffer et al. 2014, 2016). As with starspots, variations in accretion heating of the disk may still play a role, but it is unlikely to be responsible for the majority of our observed infrared variability.

Interactions between the stellar magnetosphere and the disk: the innermost extent of the gas disk is set by the stellar magnetic field, while the dust boundary is defined by where the temperature is high enough to sublimate the dust. Typically dust is truncated farther from the star than the gas, but if dust extends inward far enough, then any instabilities in the disk/magnetosphere interface could lead to infrared fluctuations. Evidence for complex structure in this region has been revealed by optical variability studies, which are sensitive to obscuration of the central star by these features. AA Tau experiences periodic occultations of the central star by a warp that is generated as the gas and dust flows onto a stellar magnetic field that is misaligned with the disk rotation axis (Bouvier et al. 2003). Similar occultation events, also called “dippers” or “AA Tau-like,” have been seen in NGC 2264 (Alencar et al. 2010) and other clusters (e.g., Ansdell et al. 2016), with rapid extinction events associated with material within the accretion flow (Stauffer et al. 2014) and longer, quasi-periodic events associated with warps in the disk (McGinnis et al. 2015). Inner warps can also be generated by massive companions misaligned with the disk, as discussed earlier, although such

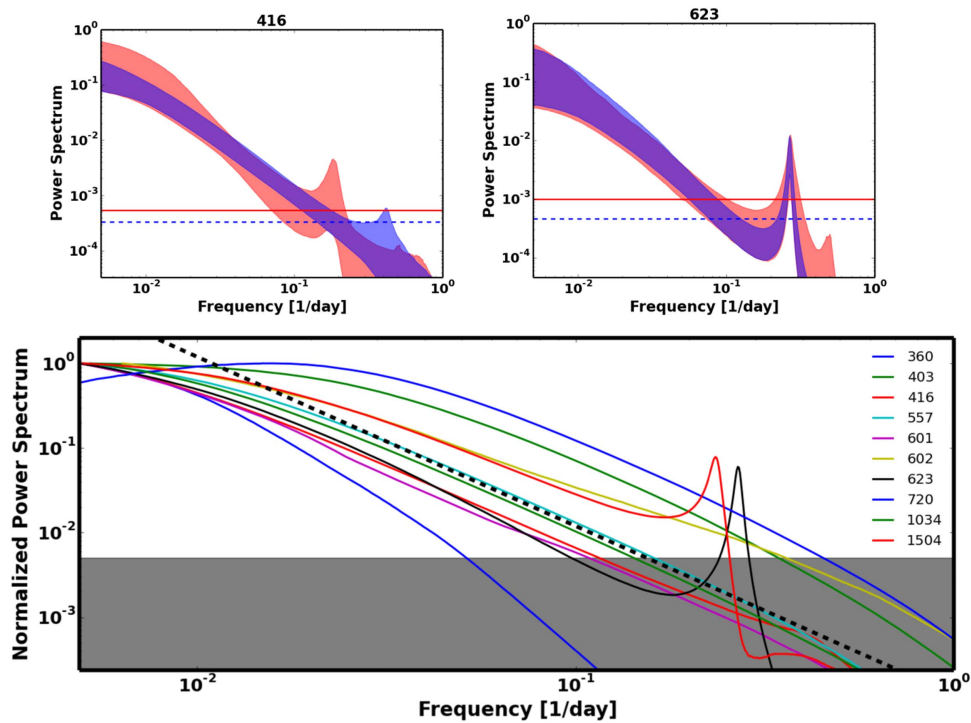


Figure 13. Top: power spectral density for stars 416 (left) and 623 (right). The red band shows the results derived from the [3.6] light curve, while the blue band shows the results from [4.5]. The band represents the 95% confidence interval of the power spectral density. Horizontal lines mark the uncertainties in the derived power spectra for [3.6] (red solid line) and [4.5] (blue dashed line). Bottom: power spectral density, normalized to their peak, derived from [4.5] for those stars with aperiodic variabilities and sufficiently sampled light curves. Only the median fit to the light curve is shown for each star. The gray band indicates the region where the uncertainties become substantial and the shape of the power spectra becomes highly uncertain. In general, the power spectra follow a $P(f) \propto f^{-2}$ shape, indicated by the black dashed line. This behavior is likely due to fluctuations arising from a range of radii within the disk.

a model has difficulty explaining the quasi-periodic nature of many of the dippers.

These structural effects can lead to changes in the infrared emission either through the increase in emitting area associated with a variable warp or through the obscuration of the stellar flux. The observed changes in [3.6]–[4.5] color fall between these two models for much of our sample. Signs of this interaction can also be searched for in the timescale of the variability. The stellar magnetic field intersects the disk at the point where the disk corotates with the star, which implies that the timescale for these interactions is the stellar rotation period. While the rotation period has not been measured for much of our sample, YSOs typically display periods of 1–15 days (Rebull et al. 2004, 2006; Cieza & Baliber 2006; Cody & Hillenbrand 2010), corresponding to corotation radii a few times the stellar radius. As a result, we expect disk/magnetosphere interactions to lead to variability that peaks on timescales of days. The exact range of timescales over which this process operates depends on the range of radii over which the disk interacts with the stellar magnetic field; a narrow (wide) range in timescales would arise if this interaction occurs over a narrow (wide) range of radii. While some of the warps can be long-lived, many are highly stochastic (McGinnis et al. 2015), leading to variations that are quasi-periodic.

This model is a promising explanation for the days- to week-long variability seen in some of our sources. As discussed earlier, stars 330 and 691 have periods consistent with stellar rotation, but amplitudes inconsistent with starspots. Extinction can produce arbitrarily large fluctuations, making the amplitudes seen in these sources consistent with periodic obscuration by a stable warp. Star 691 also has significant color variations that are consistent with reddening, supporting this scenario.

Table 5
Periodic Stars

ID	Period (days)
330	7.9
439	32
530	35
533	36
691	7.9

Note. Periods derived from the mid-infrared light curves.

While the full light curve of star 330 does not show any significant color change, by subtracting off a 50-day median-smoothed version of its light curve, we better isolate the short-timescale variability. Within this median-smoothed light curve we find a significant change in color ($\Delta[4.5]/\Delta[3.6] = 0.80 \pm 0.05$) that is consistent with reddening. In addition, star 623 has a sharp peak in its power spectrum at 3.7 days, and when phased at this period (Figure 15), the light curve exhibits a dimming feature that could be a sign of obscuration. The quasi-periodic nature of this feature may be a result of instabilities in the size of the warp. Star 1504 exhibits rapid dimming events separated by ~ 20 days, during which its color becomes redder (Figure 8). All four of these sources are consistent with quasi-periodic extinction by a disk warp close to the corotation radius.

Variations in disk/magnetosphere structure and orientation from one star to the next will influence the observed strength of this processes and may explain why disk/magnetosphere interactions are not seen more frequently in our sample. In particular, this process requires dust very close to the star. Dust

Table 6
Other Photometry

ID	This Work		Luhman et al. (2008)		Epoch	WISE Var?	NEOWISE Var?
	[3.6]	[4.5]	[3.6]	[4.5]			
75	10.94 ± 0.11	10.43 ± 0.06	10.80 ± 0.02	10.29 ± 0.02	2004 Jul 4	Y	Y
100	13.76 ± 0.03	13.27 ± 0.03	13.61 ^a ± 0.02	12.86 ^a ± 0.05	2004 Jul 4	N	N
			13.70 ± 0.02	12.88 ^a ± 0.02	2005 May 9	N	
239	7.21 ± 0.02	7.07 ± 0.01	7.08 ± 0.02	7.05 ± 0.02	2004 Jul 4	N	Y
299	9.19 ± 0.03	9.06 ± 0.02	9.05 ± 0.02	8.94 ± 0.03	2004 Jul 4	N	N
330	8.89 ± 0.09	8.51 ± 0.10	8.70 ± 0.02	8.10 ^a ± 0.03	2004 Jul 4	Y	...
360	8.22 ± 0.05	7.74 ± 0.06	8.07 ± 0.02	7.55 ^a ± 0.02	2004 Jul 4	Y	...
383	14.51 ± 0.21	13.44 ± 0.53	15.00 ± 0.13	14.43 ± 0.23
402	...	7.46 ± 0.07	saturated	saturated	2004 Jul 4	N	N
403	8.59 ± 0.11	7.85 ± 0.09	8.53 ± 0.02	7.95 ± 0.02	2004 Jul 4	N	N
416	9.65 ± 0.11	9.07 ± 0.11	9.49 ± 0.02	8.92 ± 0.02	2005 Jul 4	N	...
439	7.22 ± 0.27	6.47 ± 0.27	7.22 ± 0.02	6.51 ± 0.02	2004 Jul 4	Y	Y
530	8.30 ± 0.13	7.67 ± 0.13	8.18 ± 0.02	6.84 ^a ± 0.03	2004 Jul 4	Y	Y
533	8.99 ± 0.14	7.38 ± 0.13	8.47 ^a ± 0.02	6.97 ^a ± 0.02	2005 Jul 4	...	Y
557	12.76 ± 0.11	11.94 ± 0.13	Y	...
593	12.59 ± 0.02	12.36 ± 0.02	12.43 ^a ± 0.02	12.27 ± 0.05	2004 Jul 4	N	N
			12.42 ^a ± 0.02	12.19 ± 0.03	2005 May 9	N	...
601	7.91 ± 0.11	7.14 ± 0.10	7.90 ± 0.02	7.15 ± 0.02	2004 Jul 4	...	Y
602	10.84 ± 0.04	10.41 ± 0.06	10.66 ^a ± 0.02	10.34 ± 0.02	2004 Jul 4	N	Y
623	13.80 ± 0.08	13.21 ± 0.08	13.69 ± 0.02	13.22 ± 0.02	2004 Jul 4	N	Y
			13.67 ± 0.02	13.17 ± 0.02	2005 May 9	N	Y
691	10.90 ± 0.22	10.12 ± 0.16	11.22 ± 0.02	10.35 ± 0.02	2004 Jul 4	Y	Y
720	8.25 ± 0.09	7.71 ± 0.08	7.92 ^a ± 0.02	7.43 ^a ± 0.02	2004 Jul 4	Y	Y
791	9.47 ± 0.05	9.08 ± 0.03	9.35 ± 0.02	9.03 ± 0.02	2004 Jul 4	Y	Y
793	9.37 ± 0.07	8.75 ± 0.06	9.14 ^a ± 0.02	8.56 ^a ± 0.02	2004 Jul 4	Y	Y
966	13.00 ± 0.03	12.77 ± 0.02	12.84 ^a ± 0.02	12.72 ± 0.02	2004 Jul 4	N	Y
			12.83 ^a ± 0.02	12.65 ^a ± 0.02	2005 May 9	N	Y
1034	7.70 ± 0.13	7.32 ± 0.19	7.69 ± 0.02	7.29 ± 0.02	2004 Jul 4	N	Y
1103	8.99 ± 0.02	8.83 ± 0.02	8.76 ^a ± 0.02	8.76 ± 0.02	2004 Jul 4	N	...
1504	8.51 ± 0.09	7.92 ± 0.08	8.55 ± 0.02	8.14 ^a ± 0.02	2004 Jul 4	N	Y
2712	9.68 ± 0.03	9.56 ± 0.02	9.50 ^a ± 0.02	9.47 ± 0.02	2004 Jul 4	Y	N
4342	13.50 ± 0.05	13.01 ± 0.02	13.31 ^a ± 0.02	12.92 ± 0.02	2004 Jul 4	N	N
			13.32 ^a ± 0.02	12.98 ± 0.02	2005 May 9	N	N
5073	10.58 ± 0.03	...	10.39 ± 0.02 ^a	10.23 ± 0.03	2004 Jul 4	N	Y
			...	10.28 ± 0.02	2004 Jul 21	N	Y
6555	...	10.52 ± 0.01	10.55 ± 0.02	10.44 ± 0.02	2004 Jul 4	N	Y
8665	...	8.50 ± 0.02	8.44 ± 0.02	8.45 ± 0.02	2004 Jul 4	N	Y
14260	...	11.91 ± 0.02	11.97 ± 0.02	11.87 ± 0.02	2004 Jul 4	N	Y
			11.95 ± 0.02	11.84 ± 0.02	2005 May 9	N	Y

Notes. Comparison of the fluxes observed in our survey with those from the original Luhman et al. (2008) survey of Cha I. For data from this work we list the mean magnitude and the size of the fluctuations, as defined by the difference between the 10th and 90th percentiles. For the Luhman et al. (2008) sample we report mean magnitudes and uncertainties, as well as the date of observations, from their survey. The last two columns indicate whether the source was variable in the two short-wavelength bands of *WISE* as observed during the cryogenic *WISE* and the post-cryogenic NEOWISE missions. The *WISE* observations of Cha I spanned 2010 February–August and 2014 February–2015 August, respectively.

^a Differs significantly from the range of [3.6] or [4.5] fluxes seen in our survey.

^b No exact date for the photometry is reported.

sublimation radii are ~ 0.1 au, while typical stellar rotation periods correspond to corotation radii of ~ 0.05 au, indicating that for most stars dust/magnetosphere interactions will not produce observable effects in the infrared. Large dust grains, or a low stellar luminosity, could allow the dust to encroach on the star without sublimating, making this scenario more likely. This model also relies on a strong dipole magnetic field to create a warp, which may not be the case in all pre-main-sequence stars (Donati & Landstreet 2009) and may be less common among high-mass stars (Wade et al. 2007). Ansdell et al. (2016), using *Kepler* observations of the Upper Scorpius and ρ Ophiucus star-forming regions, primarily find “dippers” among low-mass stars. While our sample is not large enough to

search for a mass dependence, we note that stars 330, 623, 691, and 1504 are all low-mass M-type stars (Table 1). Orientation will further complicate our ability to observe a stable warp, since high inclinations are needed to generate occultation events. The average accretion rate through the disk may also play a role since the structure of the inner disk appears to vary with accretion rate (McClure et al. 2013b) and the form of the optical variability, bursts versus occultations versus spots, appears to be broadly correlated with accretion rate (Bodman et al. 2016; Sousa et al. 2016). This connection between disk/magnetosphere interactions and average accretion rate through the disk is independent of any of the infrared fluctuations induced by rapid accretion rate variability discussed earlier.

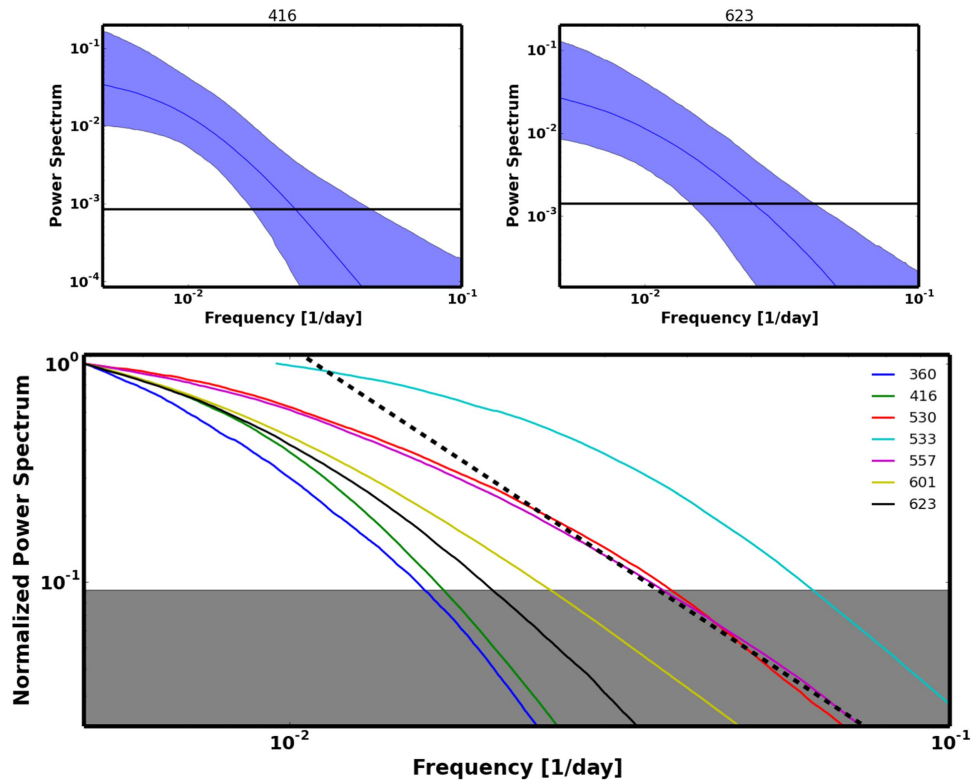


Figure 14. Top: power spectral density derived from the [3.6]–[4.5] color for stars 416 (left) and 623 (right). As compared to the [3.6] and [4.5] fluctuations, the variations in [3.6]–[4.5] are smaller, with noise limiting our ability to probe fluctuations more rapid than ~ 50 days. Bottom: power spectral density, normalized to their peak, derived from [3.6]–[4.5]. Only the median fit to the light curve is shown for each star. The gray band indicates the region where the uncertainties become substantial and the shape of the power spectra becomes highly uncertain. A $P(f) \propto f^{-2}$ shape is indicated by the black dashed line. As with the flux, the color exhibits a roughly power-law shape to its power spectrum, although the shape of the high-frequency end is unknown.

In situ perturbations of the disk: while disk/magnetosphere interactions can explain days- to week-long fluctuations, they have trouble explaining months- to year-long timescales. Accounting for the power seen at low frequencies would require a stellar magnetic field that stretches out to ~ 0.5 au, much beyond the corotation radius. Another possibility is that there are perturbations within the disk, operating at the local dynamical timescale, that lead to observable changes in the infrared emission. This could include structural perturbations, such as those generated by turbulence lifting dust away from the midplane (Turner et al. 2010), or temperature perturbations, such as collisions between massive bodies that heat up a substantial fraction of the dust, which have been seen to create significant variability among debris disks (Menu et al. 2015).

The key property in this class of models, which distinguishes it from interactions with the stellar magnetosphere, is that they can operate on a wide range of radii and hence create fluctuations in emission on a wide range of timescales. Their contribution to the power spectrum is only limited by the radii over which a particular process operates and the range of radii that generate significant [3.6] and [4.5] emission. The power-law form of the power spectral densities seen among many of the cluster members is consistent with fluctuations arising from a wide range of radii. With our well-sampled light curves, we can see that this behavior is common, suggesting that *in situ* perturbations are not restricted to a small sample of YSOs.

The color variations in much of our sample are consistent with changes in disk emission, which can arise as the structure of the hot small grains in the upper disk atmosphere rapidly varies. Poppenhaeger et al. (2015) and Rice et al. (2015) in

their surveys of IRAS:20050+2720 and Orion find that long-timescale behavior exhibits variations in color more consistent with disk perturbations. The increase in color power spectral density toward long timescales in our sample (Figure 14) is also consistent with the increased role of disk fluctuations on longer timescales. Evidence for changes in the structure of the inner disk has also been observed in pre-transition disks. These systems, with an optically thick inner disk that is separated from the optically thick outer disk by a large gap, have been observed to exhibit “seesaw” behavior in which the short-wavelength flux increases while the long-wavelength flux decreases, or vice versa (Muzerolle et al. 2009; Flaherty et al. 2012). This behavior can be explained by a variable inner disk height; as the inner disk puffs up, its own flux increases, while increasing the shadowing of the outer disk, leading to a decrease in the long-wavelength flux (Espaillat et al. 2011). Similar scale-height fluctuations may be common in less evolved systems and present at a wide range of radii, leading to the infrared fluctuations that we observe here.

In situ perturbations to disk structure are not mutually exclusive from perturbations associated with the disk/magnetosphere interface. In fact, stars 330 and 623 both show low-frequency structure in their power spectrum in addition to the more rapid behavior. Extinction may explain the rapid dimming events in star 1504, but may not explain the brightening during the middle of the light curve. If extinction operates on short timescales, while disk fluctuations operate on long timescales, the end result can be zero average change in color, as is seen in a number of sources. Which process is more evident in the power spectrum likely depends on the parameters

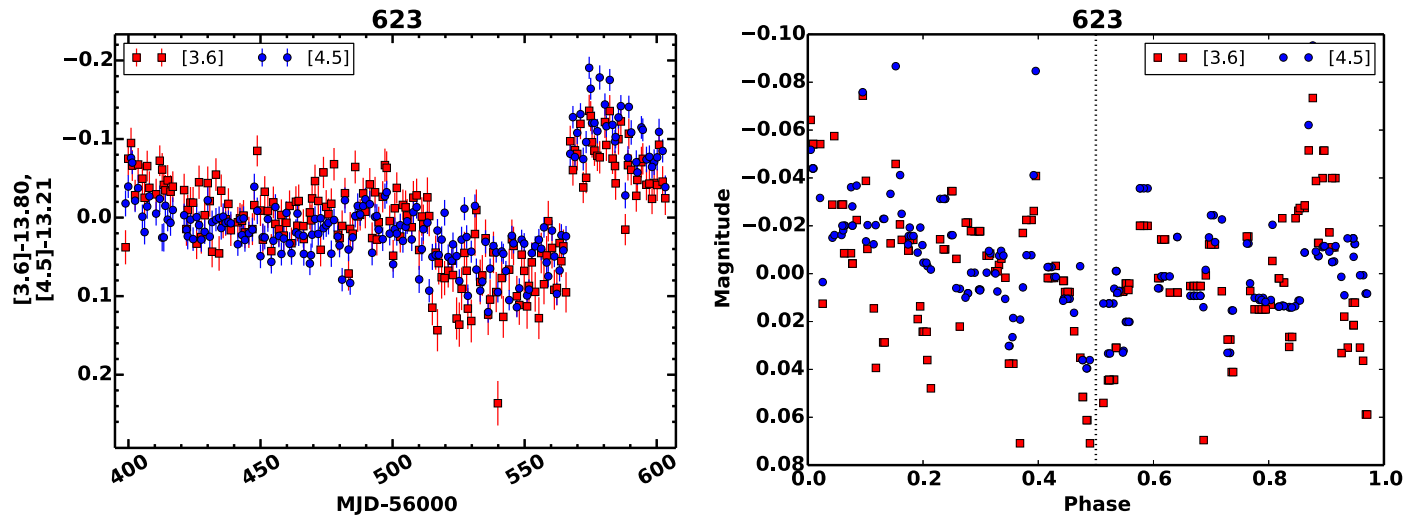


Figure 15. [3.6] (red squares) and [4.5] (blue circles) light curves for the low-mass brown dwarf OTS 44 (star 623). With a mass of $\sim 15 M_{\text{Jup}}$ it is one of the lowest-mass objects with a disk, and the lowest-mass object with known variability in its disk. The right panel shows the light curve phased to a period of 3.73 days, as indicated by analysis of the power spectrum. This phased curve has been median-smoothed over 0.1 in phase to reduce the noise and highlight the absorption feature at phase = 0.5.

of the system (stellar mass, accretion rate, etc.) and the timescales being studied in detail. Further work is needed to better understand the details of the perturbations, but our data are consistent with in situ perturbations at a wide range of radii being common among YSOs.

Beyond the dynamical timescale: in addition to the months-long variability observed during our monitoring campaign, we find evidence for longer-timescale variability, stretching out to years and decades, consistent with previous infrared variability studies covering similar timescales (Megeath et al. 2012; Parks et al. 2014; Rebull et al. 2014; Wolk et al. 2015). The models discussed above all rely on perturbations on the local dynamical timescale; to reach years would require perturbations out at 1–10 au, a region that does not contribute significantly to the [3.6] and [4.5] flux (D’Alessio et al. 2006). Instead, perturbations may be operating at the local thermal or viscous timescales. At the sublimation radius (~ 0.1 au), where the dynamical timescale is days, the thermal timescale is 1–2 yr (Chiang & Goldreich 1997), and previous models have found that thermal instabilities can generate significant changes in the physical structure of the disk (Watanabe & Lin 2008). The viscous timescale, the timescale on which significant perturbations to the surface density and accretion rate through the disk can propagate inward (Armitage 2011), is hundreds of years at ~ 0.1 au. These features are more likely to influence the very longest timescales probed, over decades of observations. More detailed characterization of the years- to decades-long fluctuations can help to probe these additional mechanisms.

6. CONCLUSIONS

Based on *Spitzer* observations of the Cha I cluster taken roughly once per day over 200 days, we find that large (0.05–0.3) infrared fluctuations are common, occurring in $\sim 80\%$ of the observed YSOs. We find that the behavior seen in previous *Spitzer* surveys, which focused on well-sampled observations over ~ 40 -day observing windows, continues to much longer timescales. In examining the properties of the variability, we find that changes in color ($\Delta[4.5]/\Delta[3.6] = 0.75\text{--}1.61$) occur in some of the YSOs and that these

fluctuations fall between the behavior expected of extinction and fluctuations in disk emission ($\Delta[4.5]/\Delta[3.6] = 0.84, 1.25$ respectively). We find a small handful of the cluster members to be periodic (5/30), including three with periods of 30–40 days, longer than the typical rotational periods of YSOs. With the combination of high cadence and long observing window, we are able to simultaneously sample both daily and months-long fluctuations. With these data, we find a smooth increase in power across two orders of magnitude in timescale in almost every YSO, with this behavior seen in the [3.6] and [4.5] fluxes and the [3.6]–[4.5] color. The shape of the power spectrum indicates that the infrared variability is largest on the longest timescales, with fluctuations ~ 2 times larger over 200 days than over the typical 40-day windows sampled by previous *Spitzer* variability surveys. A comparison of our observations with prior *Spitzer* photometry of Cha I suggests that this trend extends out to decades-long timescales.

Based on the size of the fluctuations, we can rule out the direct contribution of starspots, while perturbations from a companion are possible for the three sources with long (~ 30 -day) periods. Interactions at the disk/magnetosphere boundary can explain some of the days- to week-long fluctuations, while longer months- to year-long variability is likely a result of structural perturbations to the disk out as far as ~ 0.5 au. These processes are not mutually exclusive and can operate simultaneously within an individual system. Whichever process appears more prominent in the light curves depends on the timescales being probed, as well as the intrinsic properties of the system (e.g., accretion rate, stellar magnetic field strength, stellar luminosity). More detailed measurements of accretion rate, stellar rotation period, and inclination could further guide our understanding of which processes are strongest within a given system.

We thank the referee for the detailed report that greatly improved the manuscript. This work is based on observations made with the *Spitzer Space Telescope*, which is operated by the Jet Propulsion Laboratory, California Institute of Technology, under a contract with NASA. Support for this work was provided by NASA through an award issued by JPL/Caltech. The research made use of Astropy, a community-developed

core Python package for Astronomy (Astropy Collaboration et al. 2013). And thanks to Mary Drennan; I have not found any new stars, but there might be some new planets in here.

APPENDIX OTS 44

While many of our targets are $\sim 0.5 M_{\odot}$, our survey also includes one of the least massive known young (sub)stellar objects. OTS 44 (Luhman et al. 2004), star 623 in our sample, has a spectral type of M9.5 and is estimated to have a mass of only $\sim 15 M_{\text{jup}}$ (Bonnefoy et al. 2014). It has a strong infrared excess (Luhman et al. 2005; Harvey et al. 2012; Liu et al. 2015) and is actively accreting (Joergens et al. 2013).

OTS 44 is also variable in the infrared. In our data, the [3.6] and [4.5] emission varies by 0.15 mag over the length of our observations (Figure 15), while Luhman et al. (2008) find that the [24] flux changes from 8.81 ± 0.11 in 2004 to 9.65 ± 0.20 in 2005. While this variability is much different from the typical infrared fluctuations among field brown dwarfs that are attributed to clouds, which have timescales of a few hours and amplitudes of a few percent (Metchev et al. 2015), it is not unique among young substellar objects (Rebull et al. 2015).

The mid-infrared flux of OTS 44 slowly declines over the first 150 days, during which the color changes substantially ($\Delta [4.5]/\Delta [3.6] = 0.63 \pm 0.05$), with a stronger reddening than even that predicted for extinction. This decline is interrupted by an abrupt increase in flux that occurs between two observations, limiting its length to less than 1.6 days. Given the very low luminosity of this source, the dust sublimation radius is at 0.002 au, which has a Keplerian period of 0.2 days; such a short dynamical timescale allows for a substantial change in structure between our individual epochs and may explain the sharpness of the jump. After this abrupt increase, there is a steep decline, with fluxes almost reaching pre-outburst levels by the end of our observing campaign. The power spectrum also indicates a significant quasi-periodic feature at 3.7 days, similar to periods observed in the optical for other low-mass objects in the Cha I cluster (Cody & Hillenbrand 2014). In the smoothed light curve phased to a period of 3.7 days (Figure 15) there is evidence for a dimming feature at phase ~ 0.5 , consistent with obscuration by a clump of material at 0.016 au. In their survey of brown dwarfs in NGC 1333, Rebull et al. (2015) find one system with obscuration features that occur every 4.44 days, similar to the behavior seen here in OTS 44.

In the other observed cluster members our 200-day coverage encompasses the dynamical timescale of the inner disk, but given the small disk around this low-luminosity source, our observations extend much beyond the dynamical timescale, opening up the thermal and even viscous timescales of the disk as relevant for the gradual behavior. This allows for thermal instabilities related to variable heating of the midplane (Watanabe & Lin 2008) and perturbations to the density of inflowing material (e.g., Kelly et al. 2014) as possible explanations for the variability. Given the complexity of the light curves, it is likely that multiple processes are at play in this system.

REFERENCES

- Alencar, S. H. P., Teixeira, P. S., Guimaraes, M. M., et al. 2010, *A&A*, **519**, A88
- Ansdell, M., Gaidoes, E., Rappaport, S. A., et al. 2016, *ApJ*, **816**, 69
- Antoniucci, S., García López, R., Nisini, B., et al. 2011, *A&A*, **534**, A32
- Antoniucci, S., García López, R., Nisini, B., et al. 2014, *A&A*, **572**, A62
- Armitage, P. J. 2011, *ARA&A*, **49**, 195
- Arulanantham, N. A., Herbst, W., Cody, A. M., et al. 2016, arXiv:1602.01877
- Astropy Collaboration, Robitaille, T. P., Tollerud, E. J., et al. 2013, *A&A*, **558**, A33
- Audard, M., Ábrahám, P., Dunham, M. M., et al. 2014, in *Protostars and Planets VI*, ed. H. Beuther et al. (Tucson, AZ: Univ. Arizona Press), 387
- Baraffe, I., Homeier, D., Allard, F., & Chabrier, G. 2015, *A&A*, **577**, A42
- Basri, G., Johns Krull, C. M., & Mathieu, R. D. 1997, *AJ*, **114**, 781
- Bodman, E. H. K., Quillen, A. C., Ansdell, M., et al. 2016, arXiv:1605.03985
- Bonnefoy, M., Chauvin, G., Lagrange, A. M., et al. 2014, *A&A*, **562**, A127
- Bouvier, J., Alencar, S. H. P., Harries, T. J., Johns-Krull, C. M., & Romanova, M. M. 2007, in *Protostars and Planets V*, ed. B. Reipurth, D. Jewitt, & K. Keil (Tucson, AZ: Univ. of Arizona Press), 479
- Bouvier, J., Grankin, K. N., Alencar, S. H. P., et al. 2003, *A&A*, **409**, 169
- Carpenter, J. M., Hillenbrand, L. A., & Skrutskie, M. F. 2001, *AJ*, **121**, 3160
- Cauley, P. W., & Johns-Krull, C. M. 2015, *ApJ*, **810**, 5
- Chiang, E. I., & Goldreich, P. 1997, *ApJ*, **490**, 368
- Cieza, L., & Baliber, N. 2006, *ApJ*, **649**, 862
- Cody, A. M., & Hillenbrand, L. A. 2010, *ApJS*, **191**, 389
- Cody, A. M., & Hillenbrand, L. A. 2014, *ApJ*, **796**, 129
- Cody, A. M., Stauffer, J., Baglin, A., et al. 2014, *AJ*, **147**, 82
- Costigan, G., Vink, J. S., Scholz, A., Ray, T., & Testi, L. 2014, *MNRAS*, **440**, 3444
- Daemgen, S., Petr-Gotzens, M. G., Correia, S., et al. 2013, *A&A*, **554**, A43
- D'Alessio, P., Calvet, N., Hartmann, L., Franco-Hernández, R., & Servín, H. 2006, *ApJ*, **638**, 314
- de Vries, W. H., Becker, R. H., & White, R. L. 2003, *AJ*, **126**, 1217
- Donati, J. F., & Landstreet, J. D. 2009, *ARA&A*, **47**, 333
- Dullemond, C. P., & Monnier, J. D. 2010, *ARA&A*, **48**, 205
- Edwards, S., Kwan, J., Fischer, W., et al. 2013, *ApJ*, **778**, 148
- Emmanoulopoulos, D., McHardy, I. M., & Uttley, P. 2010, *MNRAS*, **404**, 931
- Espaillet, C., Furlan, E., D'Alessio, P., et al. 2011, *ApJ*, **728**, 49
- Findeisen, K., Cody, A. M., & Hillenbrand, L. 2015, *ApJ*, **798**, 89
- Flaherty, K. M., & Muzerolle, J. 2010, *ApJ*, **719**, 1733
- Flaherty, K. M., Muzerolle, J., Rieke, G., et al. 2012, *ApJ*, **748**, 71
- Flaherty, K. M., Muzerolle, J., Rieke, G., et al. 2013, *AJ*, **145**, 66
- Flaherty, K. M., Muzerolle, J., Wolk, S. J., et al. 2014, *ApJ*, **793**, 2
- Flaherty, K. M., Pipher, J. L., Megeath, S. T., et al. 2007, *ApJ*, **663**, 1069
- Flock, M., Fromang, S., Turner, N. J., & Benisty, M. 2016, arxiv:1604.04601
- Fragner, M. M., & Nelson, R. P. 2010, *A&A*, **511**, A77
- Frasca, A., Biazzo, K., Lanzafame, A. C., et al. 2015, *A&A*, **575**, A4
- Gramajo, L. V., Rodón, J. A., & Gómez, M. 2014, *AJ*, **147**, 140
- Günther, H. M., Cody, A. M., Covey, K. R., et al. 2014, *AJ*, **148**, 122
- Gutermuth, R. A., Megeath, S. T., Myers, P. C., et al. 2009, *ApJS*, **184**, 18
- Hartmann, L., Calvet, N., Gullbring, E., & D'Alessio, P. 1998, *ApJ*, **495**, 385
- Harvey, P. M., Henning, T., Liu, Y., et al. 2012, *ApJ*, **755**, 67
- Hawkins, M. R. S. 2002, *MNRAS*, **329**, 76
- Herbst, W., Herbst, D. K., Grossman, E. J., & Weinstein, D. 1994, *AJ*, **108**, 1906
- Hodapp, K. W., & Chini, R. 2015, *ApJ*, **813**, 107
- Ingleby, L., Espaillet, C., Calvet, N., et al. 2015, *ApJ*, **805**, 149
- Isella, A., & Natta, A. 2005, *A&A*, **438**, 899
- Jensen, E. L. N., Dhital, S., Stassun, K. G., et al. 2007, *AJ*, **134**, 241
- Joergens, V., Bonnefoy, M., Liu, Y., et al. 2013, *A&A*, **558**, L7
- Kelly, B. C., Bechtold, J., & Siemiginowska, A. 2009, *ApJ*, **698**, 895
- Kelly, B. C., Becker, A. C., Sobolewska, M., Siemiginowska, A., & Uttley, P. 2014, *ApJ*, **788**, 33
- Kim, K. H., Watson, D. M., Manoj, P., et al. 2009, *ApJ*, **700**, 1017
- Kounkel, M., Hartmann, L., Tobin, J. J., et al. 2016, arXiv:1602.05630
- Kovács, G., Zucker, S., & Mazeh, T. 2002, *A&A*, **391**, 369
- Lafrenière, D., Jayawardhana, R., Brandeker, A., Ahmic, M., & van Kerkwijk, M. H. 2008, *ApJ*, **683**, 844
- Lima, G. H. R. A., Alencar, S. H. P., Calvet, N., Hartmann, L., & Muzerolle, J. 2010, *A&A*, **522**, A104
- Liu, Y., Joergens, V., Bayo, A., Nielbock, M., & Wang, H. 2015, *A&A*, **582**, 22
- Lopez Martí, B., Jimenez Esteban, F., Bayo, A., et al. 2013, *A&A*, **551**, A46
- Luhman, K. L. 2007, *ApJS*, **173**, 104
- Luhman, K. L. 2008, in *Handbook of Star Forming Regions*, ed. B. Reipurth (Vol. II; San Francisco, CA: ASP), 169
- Luhman, K. L., Allen, L. E., Allen, P. R., et al. 2008, *ApJ*, **675**, 1375
- Luhman, K. L., D'Alessio, P., Calvet, N., et al. 2005, *ApJL*, **620**, L51
- Luhman, K. L., Peterson, D. E., & Megeath, S. T. 2004, *ApJ*, **617**, 565
- Mainzer, A., Bauer, J., Grav, T., et al. 2011, *ApJ*, **731**, 53

- Manara, C. F., Fedele, D., Herczeg, G. J., & Teixeira, P. S. 2016, [A&A](#), **585**, [A136](#)
- Manoj, P., Kim, K. H., Furlan, E., et al. 2011, [ApJS](#), **193**, [11](#)
- Mathieu, R. D., Stassun, K., Basri, G., et al. 1997, [AJ](#), **113**, [1841](#)
- McClure, M. K., Calvet, N., Espaillat, C., et al. 2013a, [ApJ](#), **769**, [73](#)
- McClure, M. K., D'Alessio, P., Calvet, N., et al. 2013b, [ApJ](#), **775**, [114](#)
- McGinnis, P. T., Alencar, S. H. P., Guimarães, M. M., et al. 2015, [A&A](#), **577**, [A11](#)
- Megeath, S. T., Gutermuth, R., Muzerolle, J., et al. 2012, [AJ](#), **144**, [192](#)
- Meng, H. Y. A., Plavchan, P., Rieke, G. H., et al. 2016, [arXiv:1603.06000](#)
- Menu, J., van Boekel, R., Henning, T., et al. 2015, [A&A](#), **581**, [A107](#)
- Metchev, S. A., Heinze, A., Apai, D., et al. 2015, [ApJ](#), **799**, [154](#)
- Millan-Gabet, R., Che, X., Monnier, J. D., et al. 2016, [arXiv:1604.06756](#)
- Morales-Calderón, M., Stauffer, J. R., Hillenbrand, L. A., et al. 2011, [ApJ](#), **733**, [50](#)
- Morales-Calderón, M., Stauffer, J. R., Stassun, K. G., et al. 2012, [ApJ](#), **753**, [149](#)
- Muzerolle, J., Flaherty, K., Balog, Z., et al. 2009, [ApJL](#), **704**, [L15](#)
- Muzerolle, J., Furlan, E., Flaherty, K., Balog, Z., & Gutermuth, R. 2013, [Natur](#), **493**, [378](#)
- Nagel, E., Flaherty, K. M., & Muzerolle, J. 2015, [ApJ](#), **808**, [147](#)
- Nguyen, D. C., Brandeker, A., van Kerkwijk, M. H., & Jayawardhana, R. 2012, [ApJ](#), **745**, [119](#)
- Nguyen, D. C., Scholz, A., van Kerkwijk, M. H., Jayawardhana, R., & Brandeker, A. 2009, [ApJL](#), **694**, [L153](#)
- Parks, J. R., Plavchan, P., White, R. J., & Gee, A. H. 2014, [ApJS](#), **211**, [3](#)
- Plavchan, P., Gee, A. H., Stapelfeldt, K., & Becker, A. 2008, [ApJL](#), **684**, [L37](#)
- Plavchan, P., Güth, T., Laohakunakorn, N., & Parks, J. R. 2013, [A&A](#), **554**, [A110](#)
- Plavchan, P., Jura, M., Kirkpatrick, J. D., Cutri, R. M., & Gallagher, S. C. 2008, [ApJS](#), **175**, [191](#)
- Poppenhaeger, K., Cody, A. M., Covey, K. R., et al. 2015, [AJ](#), **150**, [118](#)
- Rebull, L. M., Cody, A. M., Covey, K. R., et al. 2014, [AJ](#), **148**, [92](#)
- Rebull, L. M., Stauffer, J. R., Cody, A. M., et al. 2015, [AJ](#), **150**, [175](#)
- Rebull, L. M., Stauffer, J. R., Megeath, S. T., Hora, J. L., & Hartmann, L. 2006, [ApJ](#), **646**, [297](#)
- Rebull, L. M., Wolff, S. C., & Strom, S. E. 2004, [AJ](#), **127**, [1029](#)
- Reipurth, B., Clarke, C. J., Boss, A. P., et al. 2014, in *Protostars and Planets VI*, ed. H. Beuther et al. (Tucson, AZ: Univ. Arizona Press), [267](#)
- Rice, T. S., Reipurth, B., Wolk, S. J., Vaz, L. P., & Cross, N. J. G. 2015, [AJ](#), **150**, [132](#)
- Rice, T. S., Wolk, S. J., & Aspin, C. 2012, [ApJ](#), **755**, [65](#)
- Robberto, M., Spina, L., Da Rio, N., et al. 2012, [AJ](#), **144**, [83](#)
- Romanova, M. M., Kulkarni, A. K., & Lovelace, R. V. E. 2008, [ApJL](#), **673**, [L171](#)
- Scargle, J. D. 1982, [ApJ](#), **263**, [835](#)
- Scholz, A. 2012, [MNRAS](#), **420**, [1495](#)
- Siess, L., Dufour, E., & Forestini, M. 2000, [A&A](#), **358**, [593](#)
- Sousa, A. P., Alencar, S. H. P., Bouvier, J., et al. 2016, [A&A](#), **586**, [A47](#)
- Stauffer, J., Cody, A. M., Baglin, A., et al. 2014, [AJ](#), **147**, [83](#)
- Stauffer, J., Cody, A. M., McGinnis, P., et al. 2015, [AJ](#), **149**, [130](#)
- Stauffer, J., Cody, A. M., Rebull, L., et al. 2016, [AJ](#), **151**, [60](#)
- Stetson, P. B. 1996, [PASP](#), **108**, [851](#)
- Tobin, J. J., Hartmann, L., Furesz, G., Mateo, M., & Megeath, S. T. 2009, [ApJ](#), **697**, [1103](#)
- Turner, N. J., Carballido, A., & Sano, T. 2010, [ApJ](#), **708**, [188](#)
- Wade, G. A., Bagnulo, S., Drouin, D., et al. 2007, [MNRAS](#), **376**, [1145](#)
- Watanabe, S. I., & Lin, D. N. C. 2008, [ApJ](#), **672**, [1183](#)
- Windemuth, D., & Herbst, W. 2014, [AJ](#), **147**, [9](#)
- Wolk, S. J., Günther, H. M., Poppenhaeger, K., et al. 2015, [AJ](#), **150**, [145](#)
- Wolk, S. J., Rice, T. S., & Aspin, C. 2013, [ApJ](#), **773**, [145](#)
- Wright, E. L., Eisenhardt, P. R. M., Mainzer, A. K., et al. 2010, [AJ](#), **140**, [1868](#)